

## Chapter 2

# Metallic Biomaterials

Robert M. Pilliar

### 2.1 Introduction – Why Metals?

Metallic biomaterials continue to be used extensively for the fabrication of surgical implants primarily for the same reason that led to their initial selection for these devices many decades ago. The high strength and resistance to fracture that this class of material can provide, assuming proper processing, gives reliable long-term implant performance in major load-bearing situations. Coupled with a relative ease of fabrication of both simple and complex shapes using well-established and widely available fabrication techniques (e.g., casting, forging, machining), this has promoted metal use in the fields of orthopedics and dentistry primarily, the two areas in which highly loaded devices are most common although similar reasons have led to their use for forming cardiovascular devices (e.g., artificial heart valves, blood conduits and other components of heart assist devices, vascular stents), and neurovascular implants (aneurysm clips). In addition, the good electrical conductivity of metals favors their use for neuromuscular stimulation devices, the most common example being cardiac pacemakers. These favorable properties (good fracture resistance, electrical conductivity, formability) are related to the metallic interatomic bonding that characterizes this class of material. While the purpose of this chapter is to focus on the important issues pertaining to the processing and performance of metallic biomaterials and to review the metals that are currently used for implant fabrication, a brief review of fundamental issues related to the structure-property relations of metals in general follows.

Metal processing determines microstructure and that in turn determines properties (elastic constants being an exception since these are virtually structure-insensitive properties dependent on interatomic bond type and equilibrium atom packing as noted below) [1–3]. An understanding of material properties and processes used to achieve desired properties during fabrication of metallic components is critical for ensuring desired performance of implants in service. While mechanical failure is unacceptable for most engineered structures, it is particularly so for surgical implants where failure can result in patient pain and, in certain cases, death (heart valve component fracture, for example) or the need for complicated and life-threatening revision surgery.

## 2.2 Metallic Interatomic Bonding

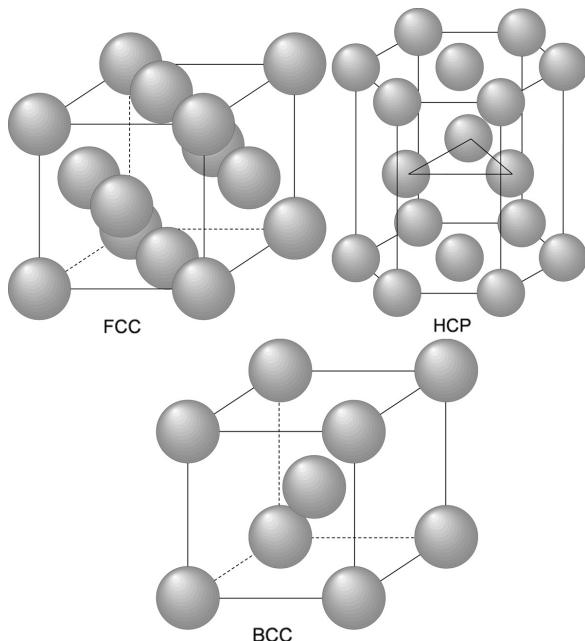
Interatomic bonding in solids occurs by strong primary (ionic, covalent, and/or metallic) and weaker secondary interatomic bonding (van der Waals and hydrogen bonding). Metals are characterized by metallic interatomic bonding with valence shell electrons forming a ‘cloud’ of electrons around the atoms/ions. This is a consequence of the high coordination number,  $N$ , (i.e., number of nearest neighboring atoms) that occur with metals (i.e.,  $N = 12$  or  $8$  for many metals). As a result of the close positioning of neighboring atoms and the shared valence electrons, the interatomic bonds are non-directional and electron movement within metal crystal lattices is easier than in ionic or covalently bonded materials. This fundamental distinguishing characteristic of metals results in the relative ease of plastic deformation (i.e., permanent deformation on loading above their yield stress) as well as the high electrical and thermal conductivities of metals. Most metals used for implant fabrication have either close-packed atomic structures with  $N = 12$  with face-centered cubic (fcc) or hexagonal close-packed (hcp) unit cells, or nearly close-packed structures with  $N = 8$  forming body-centered cubic (bcc) structures. Less commonly, tetragonal and orthorhombic as well as other unit cells do occur with some metallic biomaterials. The equilibrium distance between atoms defining the unit cells of these crystals and the strength of their interatomic bonding are determined by intrinsic factors such as atom size and valency as well as extrinsic factors (temperature, pressure). In addition to ease of deformation to desired shapes, the ability to deform plastically at high loads results in another very important feature namely an ability to blunt sharp discontinuities (through plastic deformation) thereby reducing local stress concentrations resulting in relatively high fracture toughness. As noted below, these desirable characteristics are dependent on proper selection of processing conditions for material and part formation.

## 2.3 Crystal Structures – Atom Packing in Metals

The common metallic biomaterials (i.e., stainless steel, Co-based alloys and Ti and its alloys) form either face-centered cubic, hexagonal close-packed or body-centered cubic unit cells at body temperature with ideal crystal lattice structures as shown in Fig. 2.1. Real metal crystals, in contrast to these ideal atom arrangements, contain lattice defects throughout (vacancies, dislocations, grain boundaries – Fig. 2.2). The presence of these defects, (point, line and planar defects), have a strong effect on mechanical, physical and chemical properties.

Using a simple solid sphere model to represent atom packing, arrangement of spheres in the closest packed arrangement shown in Fig. 2.3 results in either a face-centered cubic structure (2-D planar layer stacking sequence as ABCABC. . . – Fig. 2.3a), or a hexagonal close-packed structure (ABABAB. . . stacking sequence – Fig. 2.3b). The selection of the preferred arrangement for a close-packed metal depends on the lowest free energy form under given extrinsic conditions (temperature and pressure). While many metals used for implant applications form close-packed structures over a certain temperature range (e.g., Ti and its alloys are hcp

**Fig. 2.1** Unit cells for face centered cubic (fcc), hexagonal close-packed (HCP) and body-centered cubic (bcc) crystal structures (Courtesy of Scott Ramsay, Adjunct Professor, University of Toronto)



below about  $900^{\circ}\text{C}$ , Co base alloys form fcc crystalline structures above approximately  $850^{\circ}\text{C}$ , 316L stainless steel is fcc from its forging temperature  $\sim 1050^{\circ}\text{C}$  down to room temperature), others form less closely-packed structures (Ti and Ti-based alloys form bcc structures at elevated temperatures). Lowest free energy determines the most stable crystal structure under given conditions. Understanding the nature of the transformations that may occur during metal processing is important for control of properties. Phase transformations can be beneficial for achieving desired properties, but may also result in secondary phases with undesirable properties leading to unacceptable material performance. A good understanding of constitutional (equilibrium) phase diagrams is important for the design of processing methods for metallic implant formation. It should be appreciated, however, that these often over-simplified diagrams (i.e., limited to two- or three-element alloys rather than the multi-elemental compositions of most practical alloys) indicate, even for these simple compositions, equilibrium structures that may not be achieved during processing because of kinetic considerations as discussed below.

## 2.4 Phase Transformations – Diffusive and Displacive

The equilibrium arrangement of atoms in solids, as noted above, is determined by factors such as atomic size, valence, and chemical affinity between elements under specific extrinsic conditions (i.e., temperature, pressure). For given temperature and pressure conditions, the stable state is the structure of lowest free energy. Free

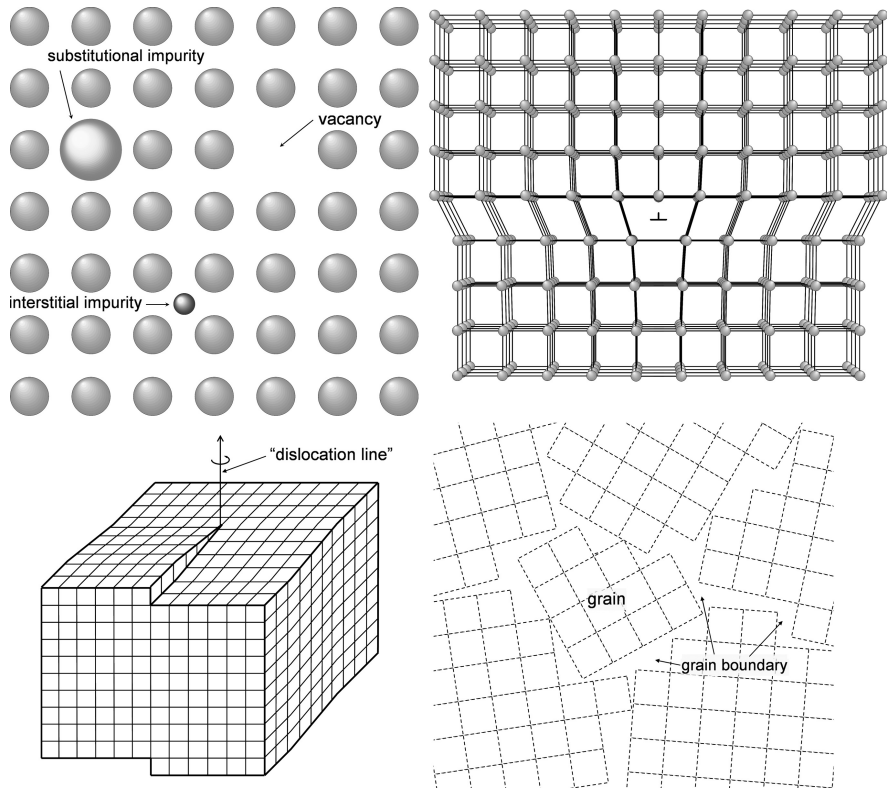


**Fig. 2.2** Crystal structures showing point defects (substitutional or interstitial elements, vacancies), line defects (edge and screw dislocations), planar defects (grain boundaries) (Courtesy of Scott Ramsay, Adjunct Professor, University of Toronto)

energy,  $G$ , is related to enthalpy,  $H$ , (heat of formation), and entropy,  $S$ , through the relation  $G = H - TS$ , where  $T$  is the absolute temperature. Changes in state or phase transformations in solids are possible if a decrease in  $G$  occurs due to the transformation (i.e.,  $\Delta G = \Delta H - T\Delta S < 0$  at the transformation temperature).

While a reduction in  $G$  represents a necessary thermodynamic condition for the formation of a new phase, atomic rearrangement to form the new phase must occur in a reasonable time period (a kinetic consideration). For most solid-state phase transformations, atom rearrangement occurs through thermally controlled diffusion processes (diffusive transformations) that result in both crystallographic and regional compositional changes within the newly formed phase(s), the amount and microstructure of the new phase(s) being dependent on temperature and time at temperature. Phase transformations can also occur through diffusionless processes that are not dependent on time at temperature but rather on temperature only or mechanical straining of samples at an appropriate temperature. These are referred to as displacive or *martensitic* transformations [4]. They are *athermal* meaning that the

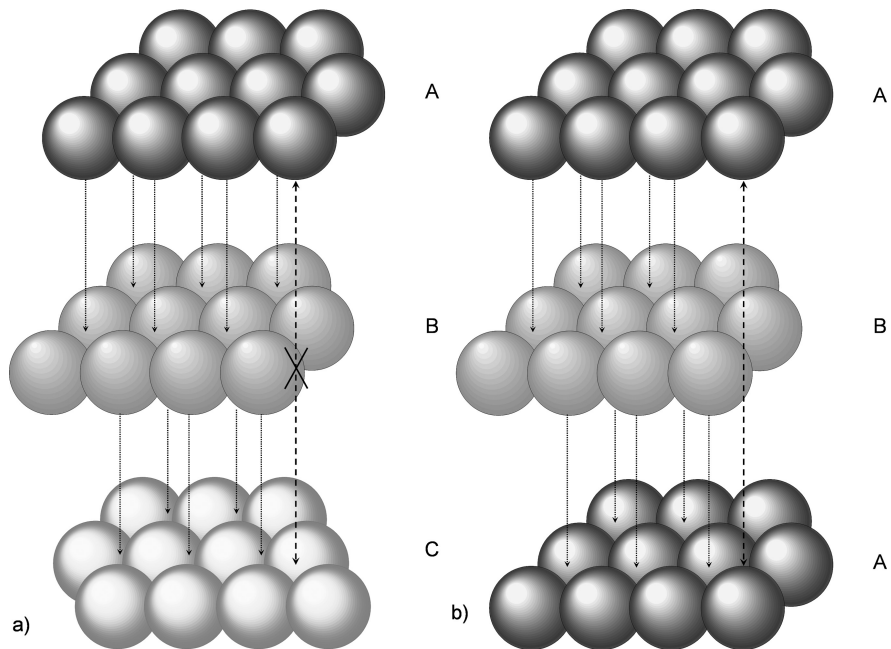


**Fig. 2.3** Solid sphere models showing the two stacking sequences possible in close-packed crystal structures. The layering sequence of the close-packed planes is different but the nearest number of neighboring atoms (coordination number) is 12 for both arrangements (Courtesy of Scott Ramsay, Adjunct Professor, University of Toronto)

amount of new phase forming from a parent phase is dependent only on the final temperature (or degree of deformation at temperature). The transformation occurs very rapidly with the transforming wave-front sweeping across the sample at a rate corresponding to the speed of sound. Very slight atom displacements are needed to achieve the transformation. The temperature at which martensite first starts to form from the parent phase (austenite) is the  $M_s$  temperature (martensite start temperature) with 100% martensite forming at the  $M_f$  temperature (martensite finish temperature). Upon heating, the reverse transformation (martensite to austenite) starts at the austenite start ( $A_s$ ) and finishes at the austenite finish ( $A_f$ ) temperatures. There is hysteresis between the forward and reverse transformation temperatures reflecting the energy required for the transformation. Displacive transformations involve very slight repositioning of atoms within a crystalline solid in combination with a so-called *lattice invariant* strain that involves lattice *twining* only in order to accommodate the overall shape change that would otherwise result from the cumulative small atom displacements. Some metallic biomaterials can transform through a displacive mechanism including the CoCrMo and Ti-based alloys that are used extensively for joint replacement implants. The Ni-Ti shape memory alloys (SMA) also transform by a displacive transformation resulting in two related phenomena that

are attracting considerable interest in biomaterials currently (i.e. the shape memory effect and superelasticity).

For Ni-Ti alloys, the net result of the austenite-to-martensite transformation is a highly twinned martensitic structure. The resulting twin boundaries are low energy boundaries that are quite mobile. Thus, components can be readily deformed at lower temperatures (where the martensite phase is stable) resulting in a change in part shape. On annealing above the  $A_f$  temperature, the martensite is transformed back to austenite *with an accompanying reversion to the initial undeformed shape*. This is referred to as the shape memory effect and can be used to advantage in bio-material applications to impart a mechanical force on tissue following implantation as the implanted device warms up to body temperature. This is described further in the section on *Ni-Ti Alloys*.

A second effect due to the martensitic transformation in Ni-Ti alloys is that of *superelasticity* (also referred to as a *pseudoelasticity*). This effect results in a very low apparent elastic modulus for the Ni-Ti alloys. It is due to the formation of *stress-induced martensite (SIM)* during mechanical deformation of the austenite phase within a limited range of temperatures just above the  $A_s$  temperature and below a temperature defined as the  $M_d$  temperature, (the maximum temperature at which stress-induced martensite will form). Mechanical strain at this temperature provides the driving force for austenite-to-martensite transformation. However, the resulting stress-induced twinned structure forms with a preferred twin *variant* (a twin formed with a twin boundary defined by a specific crystallographic plane, e.g., a {111} plane) in contrast to the formation of a family of twins having common boundary planes but differently oriented, for example having {111} boundary planes as occurs for the thermally-driven shape memory transformation. The stress-induced transformation results in a significant overall elongation in contrast to the thermally-driven one. The elongation is fully recovered on release of stress. The resulting stress-strain curve (Fig. 2.4) shows complete recovery upon unloading to relatively large strains (as high as 10% for some shape memory alloys) thereby resulting in a low apparent elastic modulus.

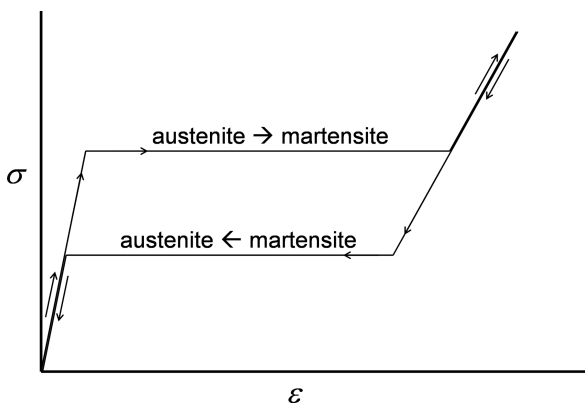


**Fig. 2.4** Stress-strain curve for a metal (such as Ni-Ti alloy) displaying stress-induced martensitic transformation and superelastic behavior. Note the hysteresis on loading and unloading

## 2.5 Diffusion in Metals

Atomic diffusion occurs during metal processing and determines the structure and properties of metallic components. Hence, solidification during casting of a melt, grain growth during elevated temperature annealing of parts, the precipitation and growth of second phase particles, sintering of metal powders to form either dense or porous structures, bonding of films or coatings to substrates, recrystallization (in which relatively strain-free crystals nucleate and grow within mechanically-deformed materials), and the formation of protective oxides over metal substrates (passive film growth) all involve atom diffusion. Thus, an understanding of atomic diffusion rates and mechanisms is important for design of processes for formation of components with desired properties. The diffusion rate,  $D$ , is given by the equation  $D = D_0 \exp(-Q/RT)$  where  $D_0$  = diffusion coefficient (characteristic of an atom diffusing in a given material),  $Q$  = activation energy for atom movement,  $R$  = universal gas constant and  $T$  = absolute temperature. This relation shows that diffusion rates fall exponentially as temperature is reduced so that at some lower temperature, diffusion driven structural changes will not occur in practical time periods even though they are energetically favored by changes in free energy (i.e.,  $\Delta G < 0$ ). As a result, metastable structures can exist at ambient temperatures. The retention at room temperature of a fcc-structured phase in Co-based alloys used for orthopedic implant fabrication is an example of this. The fcc structure ( $\gamma$ -phase) is metastable at temperatures below about 900 °C where free energy considerations would predict the formation of the hcp  $\epsilon$ -phase. Slow diffusion of Co, Cr, and Mo atoms at and below the transformation temperature prevents the ready formation of the hcp phase by a diffusive transformation. The reaction is “sluggish” and, only under special circumstances as discussed later, does the stable hcp phase form.

The formation of well-developed crystalline structures during solidification from the liquid state (or during other types of solid state formation reactions such as chemical or physical vapor deposition processes that are being used for formation of films and coatings) requires the movement of atoms to equilibrium lattice sites. Should very rapid cooling occur during solidification, such regular positioning of atoms is unable to occur and, instead, random atomic positioning and amorphous structures lacking long-range order will develop. Such amorphous structures occur more readily during solidification of complex ionically- or covalently-bonded non-metals. These have relatively lower diffusion rates due to the large molecules that define the structures of these materials and the higher activation energies for molecule movement. Some metals can also form amorphous structures on solidification but only if very high cooling rates ( $>10^6$  °C/s) are used during solidification [5]. These display some interesting properties including high hardness and excellent corrosion resistance, characteristics that are desirable for certain biomaterial applications. The high hardness can be explained by the fact that amorphous metals do not deform readily by dislocation glide as occurs with crystalline metals (see below). The excellent corrosion resistance appears related to the fact that preferred sites for initiation of corrosion reactions such as grain boundaries, dislocations, and other lattice defects (vacancies) do not exist in these structures. These as well as

nano-crystalline metals (grain size  $< 100$  nm or so) that also display interesting properties such as excellent wear resistance, high strength and corrosion resistance are discussed briefly in the *New Directions* section. These represent exciting new directions for potentially forming novel metallic implants or implant surface coatings.

## 2.6 Interatomic Forces and Elastic Moduli

### (Structure-Insensitive Properties)

All crystalline materials, as noted above, are formed with characteristic 3-D equilibrium atomic structures with specific atom arrangement/packing and equilibrium interatomic spacings that characterize that material. The interatomic forces acting on atoms in these equilibrium positions will be equal to zero as a result of a balance of attractive and repulsive force fields acting on the atoms (i.e.,  $F = dU/dr$  where  $F$  = interatomic force,  $U$  = bond energy, a function of 'r', and  $r$  = interatomic spacing – Fig. 2.5a,b). Small displacements from the equilibrium position in response to applied forces result in an increase in internal energy of the structure. The potential energy of an atom,  $U$ , can be described by an empirical equation of the form

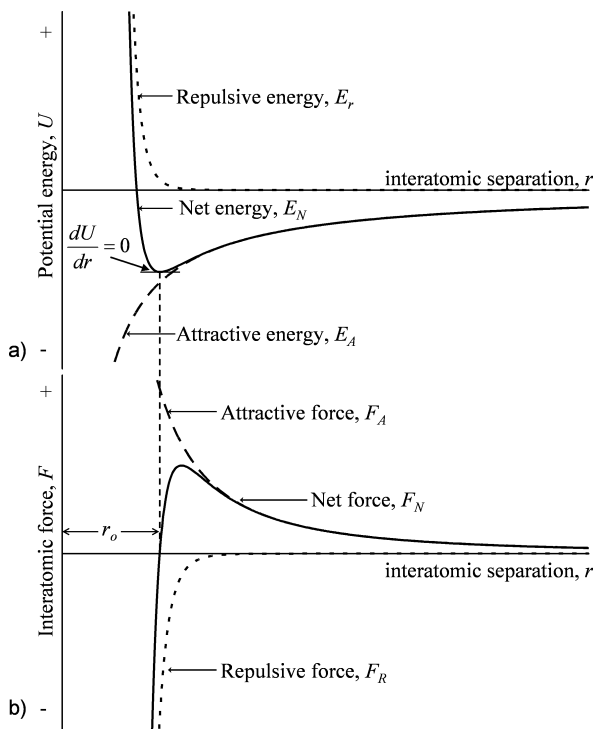


**Fig. 2.5** Potential energy vs interatomic separation curve (a) showing how the net effect of attractive and repulsive forces acting between atoms, as shown in (b), result in a potential energy minimum that defines the equilibrium interatomic separation



$U = -A/r^m + B/r^n$  where  $m < n$  [1]. The first term of this equation is related to an attractive energy force (this force is lowered as atoms are brought closer together approaching the equilibrium spacing,  $r_0$ ) while the second term is related to the repulsive force that develops as atoms are brought into too close proximity ( $r < r_0$ ). This repulsive energy term predominates at  $r < r_0$ . The interatomic force-distance relation represents an intrinsic material characteristic relating small lattice deformations (atomic displacements) and the forces resisting these displacements. Stress and strain can be determined experimentally for a material with the initial slope of the stress vs strain curve describing an intrinsic elastic constant for a material (Young's modulus,  $E$ , for very small tensile or compressive forces or Shear modulus,  $G$ , for shear forces). For small deformations in metals, the relation between stress and strain is linear and, except at higher temperatures approaching the melting temperature where atomic diffusion is rapid and creep deformation occurs, is virtually strain-rate independent for metals. Assuming a regular 3-D cubic arrangement of atoms and an applied tensile force (one tending to increase the separation between atoms), a simple estimate of  $E$  can be made [2] giving Young's Modulus,  $E = \sigma/\epsilon = dF/r_0^2/dr/r_0 = (1/r_0)(dF/dr)$  where  $\sigma$  = stress,  $\epsilon$  = strain,  $F$  = interatomic force,  $r$  and  $r_0$  = interatomic and equilibrium interatomic spacing respectively. This suggests that  $E$  is directly related to the slope of the interatomic force-distance curve and inversely proportional to the equilibrium spacing between atoms. Metal processing has very little influence on these two parameters so that elastic constants ( $E$  and  $G$ ) can be considered intrinsic material properties independent of method of processing and the resulting microstructural effects (i.e., *structure-insensitive* properties). A third elastic constant, Poisson's ratio,  $\nu$ , that describes the lateral deformation occurring as a result of axial elastic deformation ( $\nu = -\epsilon_y/\epsilon_x$ ) for a force applied in the 'x' direction) represents another *structure-insensitive* intrinsic material property. Table 2.1 summarizes some mechanical properties for a number of commonly used metallic biomaterials indicating the definite value for elastic constants in contrast

**Table 2.1** Mechanical properties of metallic biomaterials. Small variations in  $E$  may be attributable to different measuring methods. The large range of strength and % elongation to failure properties are due to different material processing. Some polymer and ceramic, as well as cortical bone properties are shown for comparison

Material	$E$ (GPa)	$\sigma_{\text{yield}}$ (MPa)	$\sigma_{\text{ult}}$ (MPa)	% elong
Fe-based	200–205	170–690	540–1000	12–40
Co-based	220–230	450–1500	655–1900	5–30
CP Ti	100–115	170–480	240–550	15–24
Ti-based	100–110	585–1050	690–1150	10–15
Ta	188	140–345	205–480	1–30
Ni-Ti (Ms)	28–41	70–140	895	~9
UHMWPE	0.5	–	~3	800
Al <sub>2</sub> O <sub>3</sub>	350–380	–	400 (flexural)	–
PS-ZrO <sub>2</sub>	200	–	800 (flexural)	–
Bone (cortical)	10–20	–	100–300	1–2

to the range of possible values for other mechanical properties. The range of these other properties is due to their dependence on material microstructure that, in turn, is a function of the method of processing used for material formation. Thus, in contrast to the elastic constants, these other properties are *structure-sensitive*. Also included in Table 2.1 are the elastic constants for some other biomaterials (polymers and ceramics) as well as bone (cortical and cancellous). The large difference in elastic constants for the metals commonly used for forming bone-interfacing implants for orthopedic applications (stainless steel, Co-based alloys, Ti and its alloys) and bone is noteworthy. This large disparity can lead to undesirable structural changes in bone situated next to a metallic implant in situations where the implants are (1) securely fastened to bone (usually a preferred situation for joint replacements and fracture stabilization) and (2) oriented with the length of the implant juxtaposing a significant length of bone (as for example a femoral hip implant stem component against the host femur). The resulting composite construct (metal implant and bone) forms, in effect, a reinforced composite so that major stresses are borne by the higher modulus metallic implant thereby ‘stress shielding’ the host bone. Because of this, disuse atrophy and significant bone loss can result over time. In addition, abnormally high stresses can develop in bone at regions where force is transferred from the implant to the host bone (e.g., at the distal tip region of the femoral stem – Fig. 2.6). Studies to develop lower elastic modulus metallic alloys to overcome this ‘stress shielding’ effect represent an active area of current biomaterials research.

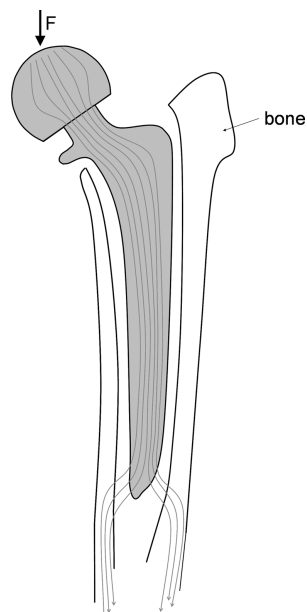


**Fig. 2.6** Schematic illustration of a securely fixed metallic femoral hip implant component in the femur showing the direction and concentration of lines of force acting during loading. The stiffer implant component acts to shield the bone next to the proximal stem portion thereby promoting bone disuse atrophy (a stress shielding effect). Note also the concentration of forces resulting in stress concentration within bone at the distal stem region (Courtesy of Scott Ramsay, Adjunct Professor, University of Toronto)

## 2.7 Plastic Deformation and *Structure-Sensitive Properties*

Metals display high degrees of ductility if appropriately processed, a direct consequence, as already noted, of the metallic interatomic bonding that allows relatively easy movement of crystal line defects (dislocations) along certain crystallographic planes (slip planes). Dislocations (edge and screw) are a type of crystal lattice defect (line defects) that occur within crystalline solids (Fig. 2.2). Their movement through the crystal lattice allows plastic deformation or yielding of metals at stress levels far below those predicted for shearing of crystal planes in idealized dislocation-free crystals. Plastic flow results in blunting of sharp geometric discontinuities that act as stress concentrators at which crack initiation will occur. The force required to cause dislocation movement or ‘gliding’ along a crystal plane is related to the strength of interatomic bonding, since dislocation movement requires sequential breakage and reformation of interatomic bonds, as well as dislocation interactions with other lattice defects (other dislocations, grain boundaries, vacancies, impurity or alloying elements). Significant dislocation movement and plastic deformation occur when stresses are above a material’s yield stress (Fig. 2.7). To increase yield strength, a number of strategies can be used all aimed at increasing a metal’s resistance to dislocation glide. These include *strain hardening* (also referred to as work hardening or cold working), alloying for substitutional or interstitial solid *solution strengthening*, *precipitation or second phase hardening*, and strengthening by *grain refinement*.

*Strain hardening* is achieved by mechanical working of a metal above its yield stress. It is a result of dislocations interacting with other dislocations during loading resulting in dislocation entanglements and pile-ups that inhibit further dislocation glide thereby resulting in higher yield stress. *Solid solution strengthening* occurs through addition of other elements to a pure metal (or through inadvertent impurity element contamination). This results in increased resistance to dislocation movement along slip planes. *Precipitation hardening or strengthening* is a result of the formation of second phase precipitates that interfere with easy dislocation

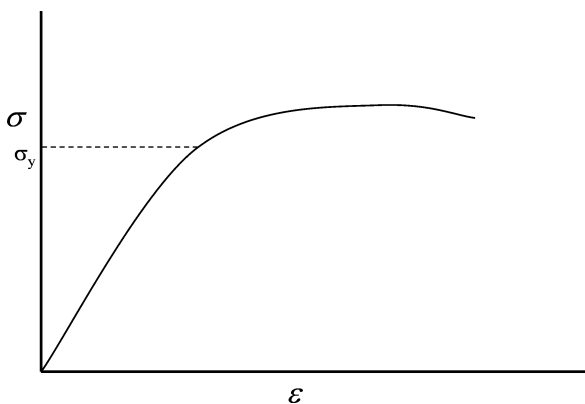


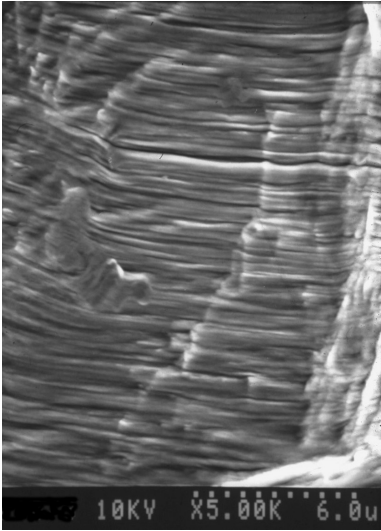
**Fig. 2.7** Stress-strain curve for a metal showing the yield stress,  $\sigma_y$ . The yield stress is normally defined as the stress corresponding to either 0.1% or 0.2% plastic strain ( $\sigma_{0.1\%}$  or  $\sigma_{0.2\%}$ )

glide. (*Dispersion strengthening* is similar but usually refers to non-metallic dispersoids within the metal matrix.) *Grain boundaries* and *interphase boundaries* also inhibit dislocation movement since glide directions along preferred slip planes must change at such junctions. Finer grain size (and consequently more grain boundary area) results in higher yield strength as described by the Hall-Petch relation ( $\sigma_y = \sigma_0 + k/d^{1/2}$  where  $d$  = mean grain size and  $\sigma_0$  and  $k$  are empirically determined constants [3]). This relation breaks down for metals with very small nano-sized or very large grains. All these possible strengthening mechanisms involve dislocation interactions with other dislocations or microstructural features. These result from processing routes used for forming implants for highly loaded applications such as those found in orthopedics and dentistry.

In addition to achieving sufficiently high yield strength to prevent unacceptable shape changes during functional loading, outright implant fracture must be avoided. Fracture can occur either as a result of a single overload event or through repeated (cyclic) loading at stresses well below the ultimate stress and even below the yield stress in the case of fatigue failure. Fatigue failure is a process resulting from the initiation and slow propagation of cracks leading to eventual catastrophic failure. This can occur in a relatively low number of cycles ( $\leq 10^4$  cycles) (high repeated strains leading to low cycle fatigue, LCF) or over millions of cycles (low cyclic strain resulting in high cycle fatigue, HCF). For the former, relatively few loading cycles are required to initiate cracks so that crack propagation rates primarily determine fatigue strength. For HCF, the number of cycles for crack initiation can represent more than 95% of the total lifetime (measured in cycles to failure). Thus, prevention of fatigue crack initiation is of crucial importance for avoiding HCF failure. Fatigue crack initiation is a result of dislocation interactions leading to formation of microvoids and dislocation run-out creating surface irregularities (slip bands) that act as stress concentrators promoting local crack initiation. Thus, processing to increase resistance to dislocation movement is a strategy for achieving higher yield strength and, hence, higher fatigue strength although yield strength increases are accompanied by reduced ductility so that an optimal degree of strengthening will normally result in the highest fatigue strength. While fatigue fractures of contemporary orthopedic and dental implants are uncommon, they do occasionally occur and often after years of apparent satisfactory implant performance and millions of cycles of loading suggesting failure due to HCF conditions. This can be confirmed by examination of fracture surfaces using high resolution scanning electron microscopy (typically at magnifications  $> 1000$  times). These studies often reveal the tell-tale signs of HCF, namely very finely-spaced fatigue striations emanating from a fatigue crack initiation site (Fig. 2.8). In general, increased fatigue strengths are related to yield strength so that the processes used to achieve increased yield strengths normally benefit fatigue strength. However, as noted above, strain hardening also results in decreased ductility which can lead to easier fatigue crack initiation so that careful selection of material processing procedures is necessary to achieve optimal static and dynamic (fatigue) properties of metallic components.

Fracture toughness ( $K_{IC}$ ) or fracture energy ( $G_c$ ) represents another important material property for consideration in device design. It is a measure of a material's

**Fig. 2.8** Scanning electron micrograph of a CP Ti dental implant that had failed as a result of fatigue. The fatigue failure is clearly identified from the striations observed on the fracture surface. Note the high magnification needed to view the striations that have an approximate 0.5  $\mu\text{m}$  spacing



damage tolerance characteristic. The ability of metals to deform plastically has a strong effect on fracture resistance since plastic deformation can result in blunting of sharp flaws thereby reducing local stress concentrations. This is the reason for the much higher fracture toughness values of metallic biomaterials compared to other high strength bioceramic materials such as  $\text{Al}_2\text{O}_3$  or phase-stabilized  $\text{ZrO}_2$  that are characterized by high compressive and much lower tensile strengths, (see Table 2.2).

Yield strength, ultimate strength, ductility, fatigue strength, fracture toughness, hardness and wear resistance are examples of *structure-sensitive* mechanical properties. Lattice defects or imperfections such as point defects (vacancies, interstitials) and planar defects (grain or crystal boundaries, twin boundaries, interphase boundaries) and the interaction of these with dislocations determine these *structure-sensitive* properties. How materials are processed determines the density of and

**Table 2.2** Metals used for orthopedic implant applications

Metal	Major/(minor) application	Processing route
Stainless steel	Osteosynthesis/(joint arthroplasty)	Hot/warm forming, machining
CoCrMo alloys	Joint arthroplasty/(osteosynthesis)	Casting, hot/warm forming, p/m
Co-Ni alloys	Osteosynthesis/(joint arthroplasty)	Hot/warm forming
CP Ti	Osteosynthesis	Hot/warm forming, machining
( $\alpha + \beta$ ) Ti alloys	Joint arthroplasty and osteosynthesis	Hot/warm forming, machining
$\beta$ /near- $\beta$ ) Ti alloys	Osteosynthesis	Hot/warm forming, machining
Ni-Ti	Osteosynthesis	Hot/warm forming, machining
Ta	Bone augmentation	Chemical vapor infiltration

interactions between these microstructural features and consequently the acceptable limits of use of components made from the materials.

## 2.8 Corrosion Resistance

Concerns over possible high rates of corrosion of metallic biomaterials and the detrimental effect that this can have on biocompatibility represent the most important consideration in the selection of metals for implant use [6]. In fact, only relatively few metals are considered acceptable for surgical and dental implant fabrication (Table 2.1). This is based on the relatively low rates of *in vivo* corrosion of these metals if properly processed. Acceptable corrosion resistance for most of these relies on their ability to form well-adhered, dense, protective oxide surface layers (passive oxide films typically 5–10 nm thick) that are retained during *in vivo* use. Thus, Ti and its alloys, Ta, CoCrMo and Co-Ni alloys, Ti-Ni alloys and certain austenitic stainless steels rely on such passive oxide layers for corrosion protection. In addition, some metals made from more noble elements that do not rely on passive film formation and that display acceptable *in vivo* corrosion properties are used for some surgical implant and dental device applications. Pt and Pt-Ir components are examples used for fabricating neuromuscular stimulation electrodes, cardiac pacemakers being the most common example. Au alloys and Pd alloys are used for dental bridge construction and as components of dental crowns (porcelain-fused-to-metal crowns). These noble metals are able to resist corrosion to an acceptable degree even in the aggressive body or oral environment due to their inherent chemical stability. Those metals that rely on passive oxide film protection, in contrast, are extremely reactive in oxygen-containing environments. This characteristic is used to advantage, for forming the well-adhering, dense oxide layers that develop either spontaneously during use or through chemical (immersion in nitric acid solution, for example), electrochemical (anodic film formation), or thermal (air oxidation) treatment as the final step in manufacture of implants from these metals. The important characteristic of these passive oxide layers is their relative stability *in vivo*, providing effective barriers to electron and ion transport. And while film growth and ion release can continue *in vivo*, the rate is sufficiently low to allow the safe use of these alloys.

## 2.9 Metals and Processes for Implant Fabrication

As already noted, only a relatively small number of metals are used currently for making surgical implants, primarily because of concerns over metal corrosion and biocompatibility. The metals used for making orthopedic implants (joint replacements and implants used in fracture repair or spinal fusion procedures) are listed in Table 2.2. These represent major load-bearing applications requiring the use of materials with sufficient corrosion resistance, strength and fracture resistance

for long-term (joint replacements) or shorter term (fracture fixation) applications. Implant loading conditions can be complex and occur in an aggressive body environment so that good corrosion-fatigue resistance is a major requirement. (Corrosion-fatigue describes the additive effect of a corrosive environment on fatigue crack initiation and propagation.) Joint replacement implants must also display good wear resistance since wear debris generated at articulating joint surfaces can either of itself or following its degradation through corrosion result in unacceptable host reactions leading to implant loosening. Ideally, joint replacement prostheses should function reliably for decades. Unfortunately, even with today's biomaterials and implant designs, this is not always the case. For implants used in fracture repair procedures the requirements are less stringent since these usually can be removed following fracture healing (i.e., after months or so) although this is not always done in practice.

The commonly used metals and some newer alloys that are being investigated currently are reviewed below. Further information can be found in other review articles on this subject [7, 8]. The focus of the present chapter is on the processing of the metallic biomaterials and how processing determines properties (i.e., fatigue strength, wear resistance, corrosion properties). The basic mechanisms outlined above are used to rationalize the process-property relations and selection of methods for implant manufacture.

## **2.10 Austenitic Stainless Steel (ASTM F 138/139, F 1314, F 1586, F 2229) <sup>1</sup>**

The stainless steel compositions (all fcc austenitic stainless steels) recommended for implant use are listed in Tables 2.3 and 2.4.

316L austenitic stainless steel (ASTM F 138/139), despite its greater susceptibility to crevice corrosion compared to other common metallic biomaterials, has over decades of use proved acceptable and the metal of choice for fracture repair devices. It has also been used for making some joint replacement components (although its use for forming these has become less common). Stainless steel's corrosion resistance is dependent on the formation of a thin Cr, Mo-containing passive surface oxide layer, the Mo imparting stability in a Cl<sup>-</sup>-containing environment. It forms a single phase (fcc austenite phase) from its forging temperature (~1050 °C) to room temperature and achieves its reasonable strength and fatigue resistance through strain hardening and solid solution strengthening mechanisms and a fine grain size. Typically, implants are forged at temperatures starting at 1050 °C and continuing through a series of forging and re-annealing steps until a near-final shape is achieved. Forging at the elevated temperature facilitates shaping since dislocation entanglements and pile-ups that would result in strain hardening at lower temperatures are eliminated. This is a result of microstructural *recovery* and

---

<sup>1</sup>American Society for Testing and Materials – recommended standards

**Table 2.3** Compositions (in wt%) of austenitic stainless steels used for orthopedic implant fabrication [7]

ASTM#	C	Mn	P	S	Si	Cr	Ni	Mo	N	Cu	Other
F 138	0.03	2.0	0.025	0.01	0.75	17.0–19.0	13.0–15.0	2.25–3.00	0.10	0.50	
F 1314	0.03	4.0–6.0	0.025	0.01	0.75	20.5–23.5	11.5–13.5	2.00–3.00	0.20–0.40	0.50	0.1–0.3Nb 0.1–0.3 V
F 1586	0.08	2–4.25	0.025	0.01	0.75	19.5–22.0	9.0–11.0	2.00–3.00	0.25–0.50	0.25	0.25–0.8Nb
F 2229	0.08	21–24	0.03	0.01	0.75	19.0–23.0	0.10	0.50–1.50	0.90 (min)	0.25	



**Table 2.4** Mechanical properties of austenitic stainless steels used for orthopedic implant fabrication; higher and lower values correspond to cold-worked and fully annealed samples respectively [7]

ASTM #	$\sigma_{\text{yield}}$ (MPa)	$\sigma_{\text{ult}}$ (MPa)	% elong	$\sigma_{\text{fatigue}}$ ( $10^7$ )
F 138	190–690	490–1350	<12–40	190–700
F 1314	380–860	690–1035	12–35	–
F 1586	430–1000	740–1100	10–35	–
F 2229	590–1550	930–1730	12–50	–

*recrystallization*, processes that occur during the elevated temperature mechanical working. (*Recovery* involves dislocation rearrangement to form lower energy networks while *recrystallization* involves the nucleation of new strain-free crystals with low dislocation density within a mechanically-worked microstructure.) Thus, easy plastic deformation and shaping (because of the low dislocation density) without the danger of component cracking are possible using elevated temperature forging. As parts cool during forging, they eventually reach the characteristic recrystallization temperature (the temperature above which nucleation of strain-free crystals occurs,  $\sim 1000^\circ\text{C}$  for stainless steel) so that continued forging on cooling below this temperature results in strain hardening of the alloy. This lower temperature ‘finish forming’ is useful for achieving a desired yield strength for the final component. The final properties (yield, ultimate strength and ductility and most importantly, fatigue strength) are dependent on the degree of ‘cold’ working that is imparted during this lower temperature mechanical deformation. Achieving a fine, uniform grain size is also important (for 316L an ASTM No. 5 grain size is recommended; i.e.,  $\sim 60\text{--}65\ \mu\text{m}$  cross-sectional dimension). Higher nitrogen content in some stainless steels (ASTM F 1314, ASTM F 1586, ASTM F 2229) results in higher strength (due to greater solid solution strengthening) as well as improved crevice and pitting corrosion resistance. The latter composition (ASTM F2229) is a Ni-free, nitrogen-strengthened austenitic stainless steel with a higher Mn content (a fcc stabilizing element like Ni) resulting in the retention of fcc austenite despite the lack of austenite-stabilizing Ni. As with the original 316L stainless steel, the corrosion resistance of all these alloys depends on the formation of a passive Cr(+Mo) oxide layer. While all these austenitic stainless steels are nominally single-phase fcc alloys, carbides can form within the structure due to the small amount of C in these alloys if they are exposed to temperatures in the  $400\text{--}800^\circ\text{C}$  range for significant periods. In this range,  $\text{M}_{23}\text{C}_6$  grain boundary phases can form (M being Cr primarily) with associated depletion of Cr from adjacent zones. The resulting denudation of Cr from regions adjacent to the carbides results in a structure that is more susceptible to intergranular corrosion because of the resulting less stable passive oxide film (due to reduced Cr content) next to the grain boundary region. This is referred to as alloy ‘sensitization’ and to minimize the possibility of its occurrence, low carbon levels are recommended for load-bearing austenitic stainless steels (hence the ‘L’ in 316L with C = 0.03 wt% maximum). An additional requirement for forming these steels

is the use of vacuum melting during solidification. This ensures low non-metallic inclusion levels. Such inclusions would act as stress concentrators thereby reducing mechanical properties (particularly fatigue strength) of components as well as making component fabrication to final shape more difficult. Following final shaping, implants are ground and polished to a desired surface finish and then given a 'passivation treatment' using a recommended procedure (e.g., exposure to a 40%  $\text{HNO}_3$  solution or thermal oxidation treatment – ASTM F 86).

Other grades of stainless steel are used to a lesser extent in other surgical implant applications [7]. These include austenitic stainless steels such as types 304 and 316 (C levels up to 0.08 for the latter as opposed to 0.03 maximum for 316L) in wire form for surgical sutures (316L is also used for this application) and for microvascular clips (for treatment of aneurysms), precipitation hardenable stainless steels (17-7 PH) and martensitic stainless steels (type 420 and 431) also for neurosurgical and microvascular clips. Austenitic stainless steels are also used for fabricating vascular stents as well as electrodes, conducting lead wires and pulse generator housings of cardiac pacing systems (304, 316, 316L alloys). The fabrication of vascular stents presents a particular challenge since these devices experience extensive change in cross-sectional dimensions during expansion to their 'working' diameter in vivo. To attain this characteristic, intricate designs that allow such extensive deformation while keeping local strains in the metal within safe limits avoiding the danger of extensive yielding and fracture have been developed. The stents can be formed to these intricate designs by laser machining fine patterns into thin-walled cylindrical tubes with highly polished surfaces [9].

## 2.11 Co-based Alloys

Co-based alloy implants can be formed by casting or forging, the latter using bar or rod stock made by conventional forming of cast billets (rolling, extrusion), or by hot isostatic pressing of Co alloy powders. Additionally, novel methods for near net-shape formation of parts from metal powders (metal injection molding or MIM [10]) are currently being explored. CoCrMo implant alloys all contain Cr (~26–30 wt%), Mo (5–7 wt%), some Ni (1 wt% maximum in order to minimize concerns related to possible Ni sensitivity), other residual trace elements (Mn, Fe, Si, N), and C (either low-C ~0.05 wt% or high-C ~0.25 wt%) (Table 2.5).

## 2.12 Cast CoCrMo (ASTM F 75)

CoCrMo alloys cast to a final form (high-C) are made by investment casting procedures (the lost wax process). This involves the simultaneous casting of a number of components (e.g., femoral stem or ball components for hip implants) onto a so-called 'casting tree' and then cutting components from the 'tree' and grinding, welding (if necessary), honing or otherwise surface finishing to achieve the final implant

**Table 2.5** Compositions (in wt%) of CoCrMo and Co-Ni alloys used for orthopedic implant fabrication [7]

ASTM #	Cr	Mo	Ni	Fe	C	Si	Mn	W	P	S	Other
F75	27–30	5–7	1.0	0.75	0.35 max	1.0	1.0	0.2	0.02	0.01	0.25 N; 0.3Al; 0.01B
F799 (low-C)	26–30	5–7	1.0	0.75	0.05	1.0	1.0	–	–	–	0.25 N
F799 (high-C)	26–30	5–7	1.0	0.75	0.25	1.0	1.0	–	–	–	0.25 N
F563	18–22	3–4	15–25	4–6	0.05	0.5	1.0	3–4	–	0.01	0.50–3.50Ti
F562 (MP35N)	19–21	9–10.5	33–37	1.0	0.025 max	0.15	0.15	–	0.015	0.01	1.0Ti
F90	19–21	–	9–11	3.0	0.05–0.15	0.40	1.0–2.0	14–16	0.04	0.03	–
F1058 (Elgiloy)	19–21	6–8	14–16	Bal	0.15	1.2	1.0–2.0	–	0.015	0.015	0.10Be; 39.0–41.0Co

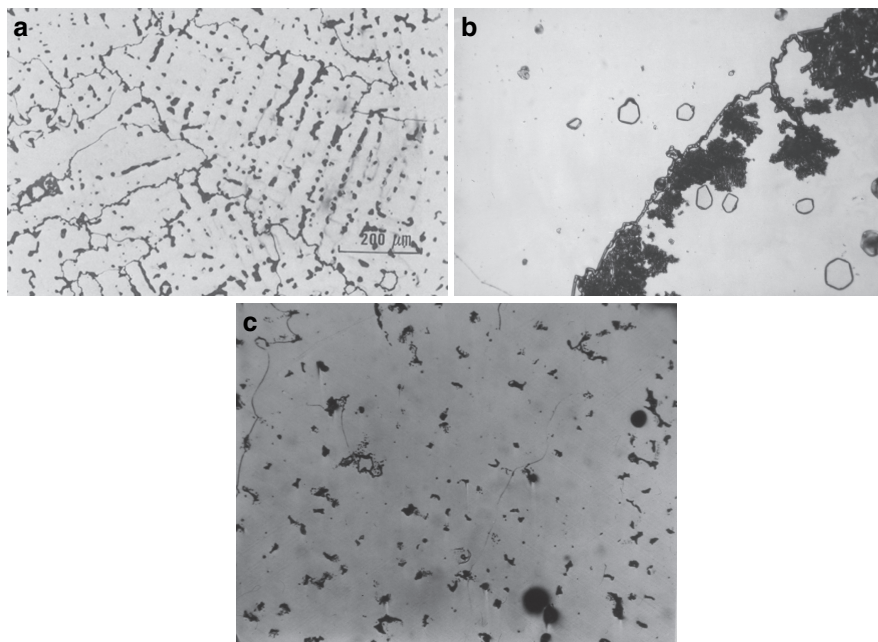


**Fig. 2.9** Scanning electron micrographs showing microstructures of (a) a polished sample of as-cast high carbon CoCrMo alloy; note the relatively large grains, the heterogeneous composition evident from the different response to chemical etching used to show the microstructure; the darkest regions correspond to carbides dispersed throughout; (b) discontinuous  $M_{23}C_6$  forming from  $\gamma$ -phase grain boundary region; (c) solution annealed CoCrMo alloy (c) showing more homogeneous structure but with some retained carbides throughout

form. The high-C alloy represents the most wear resistant clinically used metallic biomaterial, a result of the  $M_{23}C_6$  (mainly),  $M_7C_3$ , and  $M_6C$  carbides (where M is primarily Cr) that form throughout their structure during solidification (Fig. 2.9a). The alloy, after solution treatment (see below), displays a high rate of work hardening [11]. This also may contribute to the alloy's excellent wear resistance as a result of localized hardening of the surrounding Co-based matrix phase during functional loading. The alloy melts between 1350 and 1450 °C depending on its exact composition and forms a typical as-cast, cored structure on solidification with the major phase being face-centered cubic (fcc) austenite designated as either  $\gamma$ - or  $\alpha$ -phase in the literature and the interdendritic zones being enriched in Cr, Mo, and C. The  $\gamma$ -phase forms at temperatures above 890 °C while a hexagonal close-packed (hcp) structure is stable below this temperature. However, because of the sluggish nature of the fcc to hcp transformation, a metastable fcc phase is normally retained to room temperature. Subsequent aging at below 890 °C or extensive mechanical deformation temperatures below 890 °C results in the formation of either *faulted* fcc zones (*stacking faults* or regions where the ABCABC stacking sequence to form an fcc structure is altered to ABABAB stacking forming hcp zones within the fcc phase),

or hcp bands (formed by martensitic phase transformation). Aging at between 650 and 850 °C favors  $M_{23}C_6$  precipitation in the hcp zones but while this does increase yield strength, it also reduces the material's ductility to unacceptable levels, making such an aging treatment impractical [12]. As already noted, during solidification, a highly cored structure develops with interdendritic Cr-, Mo- and C-rich regions forming extensive carbide networks and other brittle intermetallic phases ( $\sigma$ -phase) that result in low ductility. (Figure 2.10 represents a pseudobinary phase diagram that predicts the formation of the heterogeneous, cored structure during normal cooling from the melt.) To homogenize partially the structure, the as-cast alloy is treated with a short ( $\sim 1$  h) solution anneal at between 1200 and 1225 °C (below 1235 °C since this corresponds to a eutectic melting temperature for the Cr-, Mo-, C-enriched interdendritic regions and heating above this temperature would result in local melting of the Cr-, Mo-, C-rich zones [13] Fig. 2.10). Following the solution anneal, the alloy is cooled rapidly through the 1100–800 °C temperature range to avoid precipitation of embrittling  $M_{23}C_6$  carbide networks. These can form as discontinuous carbide precipitates nucleated at and growing out from grain boundaries if sufficient time is allowed (Fig. 2.9b). The 1 h solution anneal treatment results in only partial homogenization of the cored structure but sufficient to give acceptable ductility (11–17% elongation). Some carbide dissolution does occur but enough of the hard carbide regions are retained to provide desired wear resistance (Fig. 2.9c). The major disadvantage of the cast and solution annealed CoCrMo alloy is its

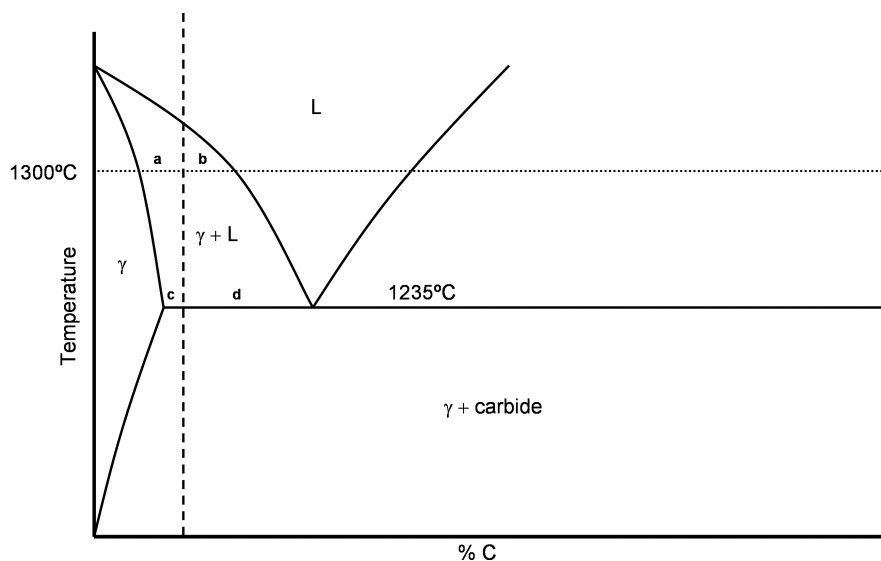


**Fig. 2.10** Pseudobinary phase diagram showing a eutectic point at 1235 °C. The vertical dashed line corresponds to an alloy with a C-content that on sintering at 1300 °C and rapid cooling would result in a:b relative ratio of carbide to  $\gamma$ -phase. Slow cooling from 1300 °C to below the eutectic temperature would result in this ratio approaching c:d (the ratio at the eutectic temperature assuming equilibrium)

**Table 2.6** Mechanical properties of CoCr and Co-Ni alloys after different treatments

Process description	$\sigma_{\text{yield}}$ (MPa)	$\sigma_{\text{ult}}$ (MPa)	% elong	$\sigma_{\text{fatigue}}$ ( $10^7$ )
<b>CoCrMo alloys</b>				
F 75 – cast + solution annealed	450–530	655–890	11–17	207–310
F 75 – cast + porous-coated	~490	~735	~11	150–207
F 799 – forged (low C)	875–995	1320–1450	19–26	670–800
F 799 – forged (low C) + P-C	~410	~815	~33	–
F 799 – forged (high C)	~1175	~1510	~10	–
F 799 – forged (high C) + P-C	600–840	1030–1280	~18	~240
P/M D-S (as-forged)	840	1280	–	690–895
P/M D-S + P-C	–	–	–	345
<b>Co-Ni Alloy (MP35N) – F 562</b>				
Annealed (1050°C)	300	800	40	340
Cold-worked (50% red in area)	650	1000	20	435
Cold-worked + aged	1900	2050	10	405
<b>Other Co Alloys</b>				
F 1058 c-w + aged (wire)	1240–1450	1860–2275	–	–
F 563 c-w + aged	827–1172	1000–1310	12–18	–

relatively low mechanical properties (other than wear resistance) (Table 2.6). This is due to the coarse grain structure (>hundreds of microns and up to the millimeter size range), inherent casting defects and shrinkage porosity resulting upon solidification and relatively slow cooling of the castings. In addition, the carbides that are retained after the solution anneal, while beneficial for wear resistance, create sites for easy crack initiation and, if distributed to form networks along grain boundaries, easy crack propagation pathways. Internal porosity (shrinkage pores) can be eliminated by hot isostatic pressing (HIP), thereby improving properties. HIP treatment has been reported to successfully improve poor quality castings but, not surprisingly, it does not significantly benefit already sound castings. However, this process does not heal surface connected defects so these can still act as preferred sites for early crack initiation. Corrosion resistance, as with the stainless steels, is dependent on the formation of a passive Cr and Mo-containing oxide. This passive oxide layer is normally formed by nitric acid solution treatment as a final step in implant manufacture (ASTM F 86).

## 2.13 Wrought CoCrMo (Low- and High-Carbon) (ASTM F 799, F 1537)

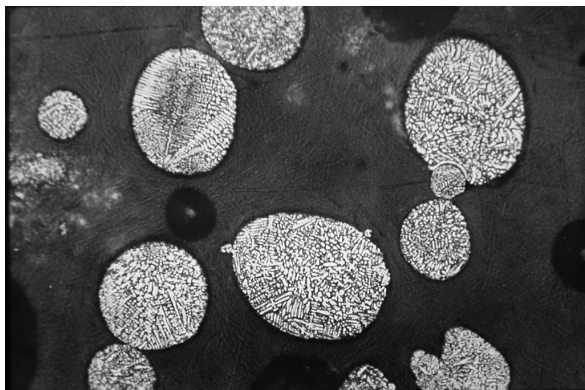
Warm or hot forging of cast CoCrMo billets can result in significantly higher mechanical properties. Such thermomechanical treatment was applied initially only to low C-containing alloys (C ~0.05 wt%). The lower carbon content results in fewer and smaller carbides throughout the structure thereby improving the alloy's

formability but at the cost of reducing wear resistance. For hot forging, billets are heated to temperatures between 1000 and 1150 °C. Re-annealing at stages during the forging process is used in order to prevent edge cracking during deformation. Final implant shapes can be achieved using closed-die forging and a series of forging and re-annealing steps. A lower temperature finish forging operation, as with the stainless steel alloys, is used to achieve a degree of strain hardening of the alloy and a final form with desirable mechanical properties. Yield, ultimate and fatigue strengths are significantly higher than for the high-C, cast alloy despite the lower carbide content. This is a result of the much finer grain size, possible stacking fault or hcp band formation, and strain hardening due to the lower temperature working operation all of which contribute to increased resistance to dislocation gliding and, hence, higher yield and fatigue strengths (Table 2.5). As noted in Table 2.6, the fatigue endurance limit for hot-forged, low-C CoCrMo alloy is greater than 600 MPa. The wear resistance of the low-C alloy is poor compared with the higher-C cast alloy thereby negating its use for femoral ball or other surface bearing components.

Closed-die forging of high-carbon CoCrMo alloys is also possible although the procedures for doing this are difficult and very close control on forging and re-annealing stages is necessary. The result is a fine-grained and strain-hardened alloy with the additional benefit of the break-up of larger carbides formed during solidification. This gives a high strength alloy with good wear resistance due to the finely distributed carbides throughout the structure. Whether cast or high-C wrought Co-based alloys provide superior wear resistance remains controversial. The fine carbide distribution does allow improved surface finishing of components and this may contribute to better wear characteristics although supporting evidence based on long term clinical comparisons has not been reported.

Fine-grained, high-C bar stock that is suitable for subsequent closed-die forging to final shape can also be formed using a *powder metallurgy* processing route. By this method, high carbon CoCrMo alloy powders are formed by atomization (either by inert gas atomization or by a rotating electrode process [8]). The powders so formed represent very rapidly solidified ‘micro-castings’ so that while retaining carbides and a cored structure (like the cast alloy), these are small and finely distributed throughout the atomized powder (Fig. 2.11). After atomization, the powders are sized by screening and then consolidated to full density by placement in a suitable containment vessel that is evacuated, sealed and hot isostatically pressed (at around 1100 °C for 1 h at 105 MPa pressure) or hot forged, to form full density CoCrMo alloy. During the period at elevated temperature, some grain coarsening occurs but it is limited in extent because of the grain growth inhibition effect of the finely distributed carbides. A dispersion strengthened powder-made alloy formed by adding La and Al to the melt stock prior to atomization resulting in additional finely-dispersed La and Al oxide particles throughout the HIP’ed alloy has been reported [14]. The rationale for introducing these finely-dispersed oxides in this case is to inhibit grain growth during a subsequent high temperature sinter anneal treatment that is used for forming a sintered porous surface coating on the implants; this process is described further in the *Surface Modification of CoCrMo Implants*

**Fig. 2.11** Scanning electron micrograph of ground and polished atomized CoCrMo powder showing the fine cored microstructure within the powder a result of the relatively rapid cooling rate during atomization



section. The containment vessel outer layer is subsequently removed from the dense compact yielding a fine-grained CoCrMo alloy containing finely distributed carbides. The fine microstructure of the resulting bar allows easier hot or warm forging to a near final form, (compared with coarser-structured alloys). Implants of relatively high strength, with good honing and polishing characteristics and good wear resistance can be formed using this metal powder-formed material.

Other novel methods such as metal injection molding (MIM) are being investigated for forming near final shapes from CoCrMo alloy powders [10]. The process involves mixing fine atomized powders with an organic binder, and extruding the resulting slurry to form pellets. These are then treated to remove the binder using a solvent and thermal decomposition during heating to the final sintering temperature that is just below the alloy's melting temperature (1340–1380 °C). (It is likely that some liquid phase contributes to sintering during this treatment as a result of localized melting of Cr-, Mo-, C-rich regions above the 1235 °C eutectic temperature). The sintered material is then hot isostatically pressed to remove any remaining porosity and annealed at just above 1200 °C to minimize carbide networks by partial carbide dissolution. This results in increased ductility.

The strengthening mechanisms for the CoCrMo alloys include solid solution strengthening, dispersion strengthening (because of the fine  $M_{23}C_6$  carbides and La and Al oxides, if present), carbide phase reinforcement [11], strain hardening (for the wrought alloys), and dislocation-grain boundary interactions. The coarse-grained cast structures exhibit ultimate and yield strengths ~860 and 550 MPa respectively with fatigue strengths ~250 MPa for samples in the solution-treated condition; fatigue strengths of 450 MPa have been reported using casting processes that result in ultrafine grain size [15]. The finer structure and strain hardening effects of the wrought alloys result in much higher ultimate tensile strengths (1330–1450 MPa), yield strengths (960–1000 MPa), and fatigue strengths ( $10^7$  endurance limit ~690–830 MPa) [15]. These values are similar to those reported for the powder-made bar stock materials formed by hot isostatic pressing (HIP) [16].



## 2.14 Surface Modification of CoCrMo Implants – Porous Coatings for Bone Ingrowth

To achieve secure implant-to-bone fixation without the use of acrylic bone cement, cast CoCrMo implant surfaces can be modified by either sintering CoCrMo powders to the bone-interfacing surfaces or plasma spray coating the surfaces [17, 18]. For the sintered coatings, typically 250–350  $\mu\text{m}$  size powders (–45/+60 mesh) are used to form porous coatings of approximately 50–70% density (i.e., vol.% porosity  $\sim$ 30–50%). Secure particle-to-particle and particle-to-substrate core bonding is achieved by sintering CoCrMo alloy powders at around 1300 °C for a period of 1 h or so. This high temperature sintering anneal significantly alters the microstructure and mechanical properties of both cast and wrought CoCrMo alloys. As noted previously for cast alloys, localized melting of the Cr-, Mo-, C-rich interdendritic zones occurs at approximately 1235 °C, the eutectic temperature for the solute-enriched interdendritic region [13]. Upon cooling, eutectic phase structures, ( $\gamma$ -phase +  $\text{M}_{23}\text{C}_6$  carbides + possibly some  $\sigma$ -phase), form inter- and intragranularly (Fig. 2.12a,b). These eutectic structures form as networks at sinter neck regions and along the solid substrate grain boundaries where they form pathways for easy crack propagation thereby resulting in reduced ductility and fracture resistance of porous-coated implants (Fig. 2.12). This undesirable effect can be minimized by slow cooling from the normal sintering temperature ( $\sim$ 1300 °C) to below the incipient eutectic melting temperature (1235 °C) [8, 18] thereby minimizing the amount of  $\gamma$ -phase + carbide eutectic formed at the eutectic temperature as predicted by the lever rule (see Fig. 2.10). While early use of sintered porous coatings was limited to cast CoCrMo compositions because of concerns of recrystallization and grain growth during sintering of wrought CoCrMo alloys leading to low strength, the development of high-C and dispersion strengthened wrought Co-based alloys with fine non-metallic dispersoids throughout that inhibit grain growth (i.e., carbides or Al and La oxides) has made it

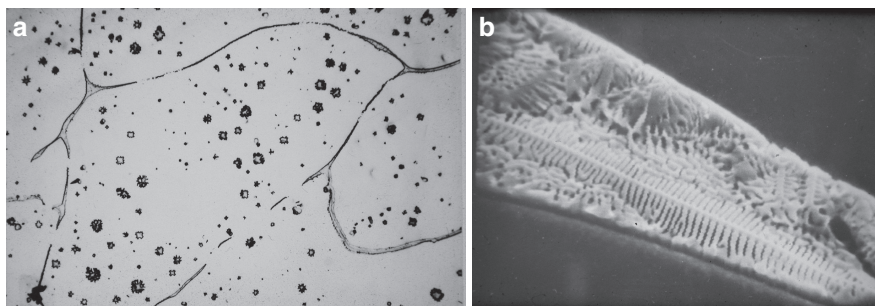


**Fig. 2.12** Scanning electron micrographs of polished CoCrMo samples following a 1300 °C 1 h sinter annealing treatment followed by a normal furnace cool to room temperature showing (a) grain boundaries with eutectic structure ( $\text{M}_{23}\text{C}_6$  +  $\gamma$ -phase primarily) and (b) higher magnification view of the grain boundary microstructure; the lamellar eutectic structure of  $\text{M}_{23}\text{C}_6$  +  $\gamma$ -phase lamellae is clearly visible

practical to porous coat these alloys and retain relatively small grains (60–150  $\mu\text{m}$  size range). Further, the more homogenous compositions of the wrought alloy substrates reduces significantly the amount of  $\text{M}_{23}\text{C}_6$ - $\gamma$ -phase eutectic formation. As a result, higher mechanical properties of wrought high-C Co alloy porous-coated samples can be achieved (fatigue strengths equal to 241 MPa compared to 207 for porous-coated cast samples [14]; La and Al oxide dispersion strengthened porous-coated alloys are reported to have higher fatigue strengths equal to 345 MPa [16]).

### **2.15 Other Co-containing Implant Alloys (ASTM F 562, F 90, F 563, F 1058)**

While the CoCrMo alloys described above represent the most common Co-based alloys used in orthopedics, other Co-containing implant alloys have been and continue to be used [7]. These are described briefly. All these contain alloying elements that significantly affect the nature of the fcc to hcp transformation of these alloys. This in turn has a strong effect on their properties. Cr, Mo, W, and Si are elements that stabilize the hcp phase while C, Ni, Mn, and Fe are fcc phase stabilizers. MP35N (F562 – Tables 2.5 and 2.6) contains 33–37 wt% Ni, an equal amount of Co and somewhat less Cr (19–21 wt%) compared with the F75 alloy. The high Ni content stabilizes the hcp phase so that at temperatures between 425 and 650  $^{\circ}\text{C}$ , a two-phase fcc ( $\gamma$ ) + hcp ( $\epsilon$ ) equilibrium structure can form. However, mechanical working and the associated strain energy is required to nucleate the  $\epsilon$ -phase at this lower temperature. The exact thermomechanical treatment used determines the size and distribution of the resulting hcp bands that form and, hence, the degree of strengthening that results due to the interaction of dislocations with the  $\gamma$ - $\epsilon$  interphase boundaries throughout the structure. To maintain acceptable corrosion resistance, MP35N has a higher Mo content than the CoCrMo alloys in order to compensate for its reduced Cr content. The higher Mo also can contribute to further strengthening of the alloy since on annealing in the 425–650  $^{\circ}\text{C}$  range, an intermetallic compound,  $\text{Co}_3\text{Mo}$  precipitates within the hcp zones. As shown in Table 2.5, the MP35N can develop very high fatigue strengths, a feature that made it particularly attractive for forming hip implant components. However, concern over its high Ni content and the reported occurrence of Ni-sensitivity in a significant percentage of the general population has limited its use for joint replacement implants although it remains popular for fabrication of fracture fixation (temporary) implants as well as conducting leads of cardiac pacing systems.

Other Co-based alloys that are used in implant applications include Elgiloy (ASTM F-1058) and the W-containing alloys (ASTM F-563) (Tables 2.5 and 2.6). Elgiloy is renowned for its high springback qualities when highly cold-worked, a property that makes it attractive for fabrication of neurosurgical and vascular implants (neural aneurysm and microvascular clamps) as well as conducting leads for pacemakers. The W-containing CoCrNi alloy (ASTM F-563) has been used for making fracture fixation implants. These alloys are not as corrosion resistant as

some of the Mo-containing Co-based alloys and they are strengthened primarily through work hardening. The common characteristic that all these Co- and CoNi-based alloys share in terms of response to thermomechanical treatment is the sluggish fcc to hcp transformation at relatively low transformation temperatures.

## 2.16 Titanium-Based Alloys

Titanium and its alloys have been used increasingly for fabrication of orthopedic implants (for fracture fixation and joint replacement) since the late 1960s. They are also used virtually exclusively for forming endosseous dental implants, another mechanically-loaded application requiring implants with good fatigue resistance characteristics. The increasing use of Ti-based metals, in addition to their good fatigue resistance, is attributed to their excellent *in vivo* corrosion resistance, a feature related to the stable passive oxide layer ( $\text{TiO}_2$ ) that rapidly forms, their lower elastic moduli compared to other metallic biomaterials (100–110 GPa compared to 200–220 GPa), and their strong osseointegration tendency (i.e., development of close bone-to-implant apposition after short implantation periods). This latter characteristic represents an important advantage for permanent bone-interfacing implants.

Pure Ti is body-centered cubic ( $\beta$ -phase) at temperatures above 883 °C (the  $\beta$ -transus temperature) and hexagonal close-packed ( $\alpha$ -phase) at lower temperatures (Fig. 2.13). Addition of most other elements stabilizes either one phase or

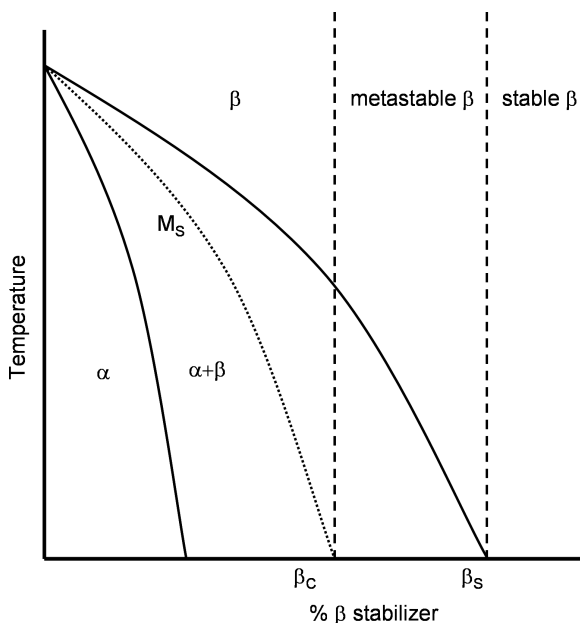


**Fig. 2.13** Ti alloy equilibrium pseudobinary phase diagram. With increased  $\beta$ -stabilizer element additions, an ( $\alpha + \beta$ ) structure develops, above  $\beta_c$  a metastable  $\beta$ -phase is possible and above  $\beta_s$  only stable  $\beta$ -phase results. The  $M_s$  line represents temperatures below which martensite can form depending on the cooling rate used

the other.  $\alpha$ -Stabilizers include Al, O, N, and C while  $\beta$ -stabilizers are of two types,  $\beta$ -isomorphous (Mo, V, Nb and Ta) and  $\beta$ -eutectoid (Fe, W, Cr, Si, Ni, Co, Mn and H) [19, 20].  $\beta$ -Isomorphous Ti alloys have attracted interest for implant applications more recently because of the low elastic moduli that are possible with these alloys if appropriately processed. The elements Zr and Sn that are found in some Ti alloys are considered to be ‘neutral’ alloying elements with no significant effect on either  $\alpha$ - or  $\beta$ -phase stabilization.

The major disadvantage of Ti and its alloys is their very poor wear resistance. This makes them unsuitable for load-bearing articulating surfaces without some type of surface modification to give greater wear resistance. This can be achieved either through ion implantation (with  $N^+$ ) or TiN film application using one of a number of physical vapor deposition (PVD) procedures. With the introduction of modular hip implant designs this has become less of an issue since, with such designs, it is possible to combine a more wear resistant bearing component made of either a Co alloy or a ceramic ( $Al_2O_3$  or Phase Stabilized  $ZrO_2$ ) with a Ti alloy stem, for example, to form a hip joint replacement with good wear and fatigue resistance. The issue, nevertheless, remains a concern since modular designs of necessity will have intercomponent junctions where relative movement and fretting can occur.

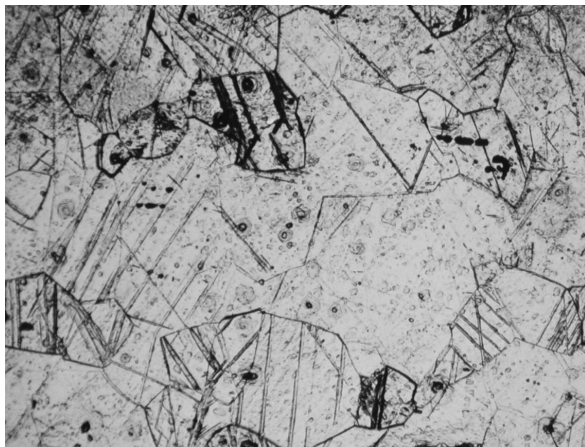
## 2.17 Commercial Purity Ti

Unalloyed Ti (commercial purity or CP Ti) can contain small amounts of interstitial elements including O, N and H. While the quantities are small (Table 2.7), they affect mechanical properties through interstitial solid solution strengthening [7]. CP Ti is available in four grades, Grade I having the lowest O content and yield strength but highest ductility and Grade IV the highest O content and strength but lowest ductility. The Grade III and IV types are used for fabricating implants for use in osteosynthesis (fracture repair and spinal fusion) but the mechanical strength (low fatigue strength in particular) precludes their use for joint replacement prostheses. CP Ti is used, however, for endosseous dental implants where its characteristic of promoting rapid osseointegration makes it particularly attractive. This is believed to be due to  $OH^-$  ion incorporation within the passive  $TiO_2$  layer and reaction of the resulting hydroxylated surface zone with bone mineral phase constituents ( $Ca^{2+}$  and  $(PO_4)^{3-}$ ). Strain hardening during mechanical forming of parts, its fine grain

**Table 2.7** Interstitial element limits and mechanical properties for CP Ti (Grades 1–4)

Grade	O (max)	N (max)	H (max)	$\sigma_{yield}$ (MPa)	$\sigma_{ult}$ (MPa)	% elong
1	0.18	0.03	0.015	170	240	24
2	0.25	0.03	0.015	275	345	20
3	0.35	0.05	0.015	380	450	18
4	0.40	0.05	0.015	483	550	15

**Fig. 2.14** Scanning electron micrographs of CP Ti. The structure is single phase. Grain and twin boundaries can be seen



size, and interstitial solid solution strengtheners such as oxygen and nitrogen are responsible for strengthening CP Ti (Fig. 2.14).

## 2.18 ( $\alpha + \beta$ ) Ti Alloys

Alloying of Ti is used to form a two-phase ( $\alpha + \beta$ ) alloy of higher strength (yield, ultimate and fatigue) than CP Ti while maintaining excellent corrosion resistance and osseointegration tendency, again because of the  $\text{TiO}_2/\text{OH}$  surface film that rapidly forms.

The ( $\alpha + \beta$ ) Ti alloy with the longest history of use for major load-bearing applications is Ti6Al4V alloy with Ti6Al7Nb and Ti5Al2.5Fe being more recent alternatives that are similarly processed giving similar properties. All three alloys behave equally well in clinical use. Bar stock of these alloys is formed by thermo-mechanical processing (mill-annealing) giving high fatigue strength materials (Table 2.8). Combined with their excellent corrosion resistance, implants made from these alloys display superior corrosion-fatigue properties compared to other metallic biomaterials. The mechanical properties of the ( $\alpha + \beta$ ) Ti alloys, fatigue strength in particular, are strongly dependent on size and distribution of the  $\alpha$  and  $\beta$  phase regions [8]. The so-called mill-annealed treatment (see below) results in the formation of small, equiaxed  $\alpha$  grains surrounded by  $\beta$ -phase particles (Fig. 2.15a). This microstructure (developed initially for aircraft/aerospace applications) results in superior fatigue crack initiation resistance and excellent high cycle fatigue strength. The mill annealing process involves mechanically working the alloy to desired form at a temperature just below the  $\beta$ -transus temperature, rapid cooling (water quenching) to room temperature and then annealing to recrystallize the worked structure at around 750 °C (i.e., well within the  $\alpha + \beta$  two-phase field). The rapid quenching treatment results in the formation of  $\alpha$ , and a metastable

**Table 2.8** Mechanical properties of Ti alloys

Alloy	E(GPa)	$\sigma_{\text{yield}}$ (MPa)	$\sigma_{\text{ult}}$ (MPa)	% elong	$\sigma_{\text{fatigue}}$ ( $10^7$ )
<b><math>\alpha</math>-<math>\beta</math> Alloys</b>					
Ti-6Al-4 V	110	860	930	10–15	610–625
Ti-6Al-7Nb	105	795	860	10	500–600
Ti-5Al-2.5Fe	110	820	900	6	580
<b><math>\beta</math>/Near-<math>\beta</math> alloys</b>					
Ti-12Mo-6Zr-2Fe (TMZF)	74–85	1000–1060	1060–1100	18–22	525
Ti-15Mo-2.8Nb-0.2Si-0.26 (21SRx)	83	945–987	980–1000	16–18	490
Ti-35.5Nb-7.3Zr-5.7Ta (TNZT)	55–66	793	827	20	265
Ti-13Nb-13Zr	79–84	863–908	973–1037	10–16	500

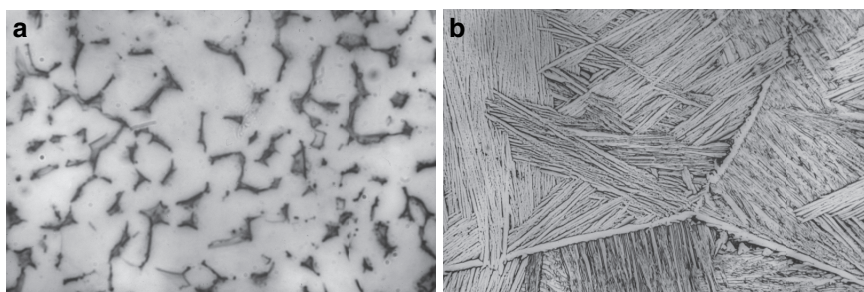


**Fig. 2.15** Microstructure of Ti6Al4V alloy; mill-annealed condition (a) – light regions are  $\alpha$ -phase and darker zones are  $\beta$ -phase regions;  $\beta$ -annealed condition (b) showing the lighter appearing  $\alpha$ -lamellae separated by  $\beta$ -phase lamellae. Note also the domain structures (zones within a single grain with  $\alpha$  to  $\beta$  formed on different habit planes, i.e., same  $\alpha$  to  $\beta$  orientation relation but involving planes in a different crystallographic orientation)

$\alpha'$ -phase as well as the retention of some  $\beta$ -phase;  $\alpha'$  forms by a martensitic transformation mechanism. The 750 °C anneal, in addition to recrystallizing the worked structure, also results in the transformation of  $\alpha'$  to the stable  $\alpha$ -phase. The amounts of  $\alpha$  and  $\beta$ , as well as the size and distribution of these phases is dependent on the extent of mechanical deformation during component forming at near the transus temperature, the exact forming temperature and the recrystallization treatment. Fatigue strengths greater than 650 MPa ( $10^7$  endurance limit) can be achieved.

The excellent corrosion resistance of Ti6Al4V makes it an attractive choice for forming high surface area, porous-coated or other surface-textured orthopedic implants either by sintering Ti or Ti alloy powders or fibers to the surface of machined substrates or by plasma spray deposition of Ti. Porous coatings formed by sintering the Ti-based materials involve sintering in a high vacuum or other non-oxidizing atmosphere at temperatures above 1250 °C for 1 h or so followed by furnace cooling to room temperature. This so-called  $\beta$ -anneal treatment results in a microstructure consisting of a lamellar ( $\alpha + \beta$ ) structure with ‘colonies’ of lamellae forming within prior  $\beta$  grains (Fig. 2.15b). Because of the higher annealing

temperature within the  $\beta$ -phase field (more than 250 °C above the  $\alpha$ - $\beta$  transus temperature), large  $\beta$  grains form. The ‘colonies’ that form throughout the structure represent zones in which the  $\alpha$  and  $\beta$  lamellae are oriented in different directions but all with a common crystallographic  $\alpha$ -to- $\beta$  orientation relation (i.e., lamellae form on common ‘habit’ planes in the different colonies). The presence of these colonies and colony boundaries contributes to the strengthening of the alloy. However, the fatigue strength of the  $\beta$ -annealed samples is lower than for mill-annealed samples (i.e.,  $10^7$  fatigue endurance limit of smooth-surfaced  $\beta$ -annealed samples  $\sim 550$  MPa compared to 620 MPa for mill-annealed samples [8, 21]). Of far greater consequence to fatigue strength is the effect of the porous coating per se [21]. It results in a reduction of fatigue strength to about a third (i.e., from 600 MPa to approximately 200 MPa). This is due to the notch fatigue sensitivity of hcp metals in general and specifically to Ti and other  $\alpha$ -phase-containing Ti alloys. The sinter neck-substrate junctions of the sintered porous layer represent stress concentrators at which fatigue can readily initiate. Design and use of porous-coated Ti6Al4V components must take into consideration this reduced fatigue strength. Some femoral hip stem components are made with porous coatings on all but the lateral stem surface since the highest tensile stress (stresses primarily responsible for fatigue crack initiation) is expected to occur at this surface during normal functional loading of implants. Plasma spray deposition of Ti to form a textured surface suitable for cementless implant fixation is possible without significantly altering the mill-annealed implant core microstructure since the temperature within the alloy bulk remains low. Nevertheless a similar reduction in fatigue strength does occur since the resulting surface is irregular with many sites of surface stress concentration.

## 2.19 $\beta$ -Ti and Near $\beta$ -Ti Alloys

These alloys have higher levels of  $\beta$ -stabilizing elements, Mo displaying one of the strongest effects. A number of  $\beta$ -Ti alloys that have been developed for use in orthopedic implants are listed in Table 2.8. These alloys are characterized by a Mo equivalent  $>10$ . This is calculated by using different weighting factors for the elements added in forming the Ti alloy (i.e., Mo equiv = 1.0 (wt% Mo) + 0.67 (wt% V) + 0.44 (wt% W) + 0.28 (wt% Nb) + 0.22 (wt% Ta) + 2.9 (wt% Fe) + 1.6 (wt% Cr) + ... [22]). While the Young’s moduli of Ti and the ( $\alpha$  +  $\beta$ ) Ti alloys are significantly lower than those of CoCrMo or stainless steel alloys ( $\sim 110$  compared to 220 and 200 GPa respectively), they nevertheless are 5–10 times greater than the modulus reported for cortical bone (10–20 GPa). The issue of stress shielding of bone next to well-fixed CP Ti or ( $\alpha$  +  $\beta$ ) Ti alloy implants is a concern in the case of long-term load-bearing implant use (although less so than with the higher modulus Co-based or stainless steel alloys). The  $\beta$  and so-called near- $\beta$  Ti alloys if appropriately processed exhibit significantly lower elastic moduli (values as low as 44–51 GPa for water-quenched and cold-worked Ti-13Nb-13Zr, a near- $\beta$  alloy [23]). These alloys if appropriately processed display good formability, high hardenability,

excellent corrosion resistance, and better notch sensitivity than the  $(\alpha + \beta)$  Ti alloys. Annealing results in higher strength as a result of precipitation strengthening but this also results in an increase in modulus [20].

$\beta$ -Ti alloys are characterized by retention of 100%  $\beta$ -phase on cooling from above the  $\beta$ -transus [22]. Considering the pseudobinary phase diagram of Ti +  $\beta$ -stabilizer alloying additions (Fig. 2.13), a metastable  $\beta$ -phase is retained on cooling from above the  $\beta$ -transus if the  $\beta$ -stabilizer content is greater than  $\beta_c$  and less than  $\beta_s$ . For levels greater than  $\beta_s$ ,  $\beta$ -phase represents the equilibrium structure. The metastable  $\beta$  structures are characterized by low elastic modulus (55–75 GPa) but relatively low fatigue strength (e.g.,  $10^7$  fatigue endurance limit  $\sim 265$  MPa for the Ti-35Nb-5Ta-7Zr alloy (TNZT) (Table 2.8). As noted above, annealing the metastable  $\beta$  in the two-phase  $(\alpha + \beta)$  field region results in some  $\alpha$ -phase precipitation and an increase in strength but also a rise in elastic modulus to values approaching or just above 100 GPa (dependent on the amount of  $\alpha$ -phase that forms).

Ti-13Nb-13Zr is an example of a so-called near  $\beta$ -Ti alloy [23]. Rapid cooling (water quenching) this alloy results in suppression of the  $\beta$ -transus temperature to a low enough temperature ( $< 575^\circ\text{C}$ ) to cause formation of acicular  $\alpha'$  martensite, an hcp phase formed by a displacive transformation. This structure is characterized by a Young's modulus  $\sim 64$ –77 GPa (Table 2.8). Subsequent annealing in the  $(\alpha + \beta)$  two-phase field ( $500^\circ\text{C}$  for 6 h – an aging heat treatment) causes the acicular  $\alpha'$  to coarsen and fine  $\beta$ -phase precipitates to form throughout, resulting in higher strength (because of precipitation strengthening) with an associated increase in elastic modulus to about 81 GPa. Heavy cold-working of  $\alpha'$  martensite is possible and results in the formation of a lower modulus material ( $\sim 45$  GPa) with strength even greater than water-quenched and precipitation hardened material while maintaining good ductility. Surface hardening for improved wear resistance can be achieved by aging (at  $500^\circ\text{C}$ , for example) in an oxygen-containing environment [23]. This is due to the formation of a hard surface oxide layer as well as interstitial solid solution strengthening of the subsurface region (diffusion hardening).

## 2.20 Zr-Nb Alloy

Zirconium, like titanium, is a highly reactive metal and will form a dense cohesive surface oxide layer ( $\text{ZrO}_2$ ) spontaneously on exposure to an oxygen-containing environment. In addition to the resulting corrosion protection,  $\text{ZrO}_2$  is very hard and can be used to form a good wear resistant surface assuming sufficient layer thickness. A Zr-2.5Nb alloy, developed initially for nuclear industry applications, when annealed in an oxygen-containing atmosphere at  $500^\circ\text{C}$  develops a relatively thick ( $5\ \mu\text{m}$ ) monoclinic  $\text{ZrO}_2$  layer over the alloy substrate [24]. The underlying alloy consists of a two-phase  $(\alpha + \beta)$  structure with the dominant phase being hcp  $\alpha$  with a small percentage of bcc  $\beta$  phase distributed throughout. Following the  $500^\circ\text{C}$  surface oxidation treatment, the sub-oxide alloy zone is also hardened through oxygen diffusion into the lattice (interstitial solid solution strengthening). Surface oxidized



Zr-Nb alloy is used for making orthopedic components that are primarily intended for compressive loading and resisting wear (such as femoral hip implant and knee implant components). The structure offers the advantage over whole ceramic components such as  $\text{Al}_2\text{O}_3$  or phase-stabilized  $\text{ZrO}_2$  of reducing risks of catastrophic fracture as a result of rapid crack initiation and propagation within the ceramic phase since the  $\text{ZrO}_2$  layer is reinforced by a Zr-Nb alloy body. Clinical outcomes of implants using this novel system are being followed with great interest.

## 2.21 Ni-Ti Alloys (Nitinol)

The equiatomic Ni-Ti alloy (Nitinol) is used currently in orthopedic, dental and cardiovascular applications [25]. The shape-memory effect that the alloy displays as well as its reported good corrosion resistance (the result of a  $\text{TiO}_2$  passive surface layer) and its pseudoelastic property ( $E \sim 28\text{--}41$  GPa for the martensitic phase) has attracted considerable interest in the biomaterials field in recent years. In vivo studies have indicated that the material is biocompatible despite its high Ni content [26, 27]. However, the concern over long-term consequences of even minor amounts of Ni ion released are likely to limit its use. Published reports indicate that with proper processing, corrosion properties comparable to 316L stainless steel are achievable [28–30] so that use in limited term applications such as fracture fixation is practical.

The shape memory effect is due to the thermoelastic martensitic transformation that occurs with the Ni-Ti shape memory alloys. Cooling from a high temperature (i.e., above body temperature for some Ni-Ti-based alloys), to a lower temperature results in the transformation of the austenite phase (an ordered intermetallic compound with a distorted bcc unit cell structure – a result of the ordering of Ni and Ti atoms giving a so-called B2 unit cell structure) to martensite. The transformation is isothermal with most of the phase change occurring over a fairly narrow temperature range between  $M_s$  and  $M_f$ . The temperature at which the austenite-to-martensite (or reverse) transformation occurs is dependent on the exact composition of the alloy. The Ni-Ti intermetallic compound, unlike most other intermetallic compounds, has a moderate range of solubility for excess Ni or Ti as well as other elements and this allows ‘engineering’ of the critical transformation temperatures ( $M_s$ ,  $M_f$ ,  $A_s$  and  $A_f$ ). Thus, it is possible to develop shape memory alloys (SMAs) with transformation temperatures corresponding to body temperature. The austenite-martensite transformation can also be induced by mechanical deformation. While the overall change in shape due to cooling of austenite is minor due to the formation of a number of counteracting twin variants that develop thereby minimizing the overall shape change, as discussed previously, stress-induced martensite results in the development of a preferred twin variant. This involves a so-called *detwinning* reaction in which a twin variant preferentially oriented in the principal strain direction grows at the expense of other twins resulting in significant volume and net shape changes. If this shape change is constrained, appreciable stress can develop in the material

and this stress can be transferred to adjacent tissues, for example, (assuming secure anchorage of tissue to the Ni-Ti component). By way of example, a fracture fixation staple made of Nitinol, if deformed in the martensitic state (i.e., at room temperature) and then used to unite fractured bone fragments, will exert a strong force pulling the fragments together as it warms up in the body to above its  $A_f$  temperature and reverts to its prior austenitic shape. Other applications have been proposed in orthopedics including other fracture fixation devices, spinal rods for treatment of scoliosis, cages for use during spinal fusion and even self-locking joint replacement components [29].

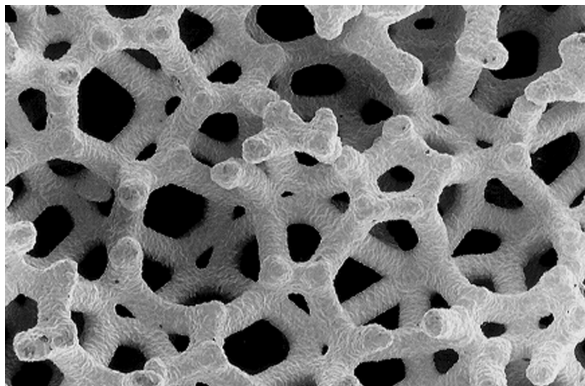
Wires formed of Nitinol are used currently in orthodontics although, in this application it is the alloy's pseudoelasticity that makes it so attractive. SMAs are also used for cardiovascular stents where the pseudoelastic feature facilitates stent expansion/deployment following insertion into an artery. The ability to tailor the transformation temperature of Ni-Ti alloys through slight alloying modifications as noted above is important since this allows the formation of materials and devices displaying this superelastic behavior at a desired temperature corresponding to expected in-service conditions. Orthodontic wires formed from a Ni-Ti-based alloy are useful because of the large 'working range' that these wires provide during force application for tooth re-positioning.

The stress-strain curves for NiTi alloys are dependent on the  $M_s$  temperatures with yield strengths and fatigue strengths increasing with decreasing  $M_s$ . Accurate determination of alloy transformation temperatures is critical for the design of components and prediction of performance.

## 2.22 Tantalum

Porous tantalum foam structures are used as bone augmentation templates. Ta has been considered for many years to be biocompatible as a result of the stable tantalum oxide ( $Ta_2O_5$ ) that forms on its surface. The metal has a long history of use in other implant applications such as implantable cranial plates. Ta foam structures for bone augmentation use [31] are formed by chemical vapor deposition (CVD) and infiltration (CVI) of tantalum onto vitreous carbon lattice structures, thereby building up Ta struts of desired dimensions. The vitreous carbon lattices are formed by pyrolysis of thermosetting polymer foams. The Ta is deposited onto the carbon filamentous structure to a desired thickness giving an open-pored Ta structure (approximately 99 wt% Ta + 1 wt% vitreous carbon) (Fig. 2.16). The dimensions of the Ta struts are controlled by the amount of Ta applied and this determines the mechanical properties of the foam. Structures with compressive and tensile strengths  $\sim 60$  and  $63$  MPa respectively and compressive fatigue strengths  $\sim 23$  MPa ( $5 \times 10^6$  endurance limit) have been reported [31]. Continuous interconnecting pores, or cells, about  $550 \mu\text{m}$  in size, are formed and elastic and strength properties similar to those of cancellous bone result. Animal studies [32] have demonstrated the effectiveness of these structures for bone augmentation purposes. While the as-made mechanical properties of the foams are low, they are considered sufficient to allow bone ingrowth and filling

**Fig. 2.16** Scanning electron micrograph of open-pored Ta foam (courtesy Dr JD Bobyn, McGill University, Montreal, Canada)



of the structures after which bone is expected to eventually satisfy the load-bearing requirements.

## 2.23 Platinum, Platinum-Iridium

Electrodes used for neuromuscular stimulation require the use of materials that are corrosion resistant under extreme voltage potential and charge transfer conditions. The noble metals (Pt and Pt-Ir alloys) satisfy these conditions and are the principal materials used for making electrodes for electrical stimulation and sensing purposes. The Pt-Ir alloys (10–30 wt% Ir) offer the advantage of higher mechanical properties (scratch resistance) compared with unalloyed Pt because of solid solution strengthening. Other possible noble metals that have been used for fabricating electrodes for electrical stimulation include rhodium, gold and palladium but these are not used extensively [7]. Some non-noble metals have also been used (stainless steel, Ti, Co-based alloys) but these are more prone to corrosion (passive film breakdown occurs at potentials above the breakdown potential). Hence, these alloys are not as suitable as the noble metals.

Conducting leads used with the electrodes are made of metals that, in addition to being corrosion resistant and electrically conductive, must display good flexural fatigue strength. Helically coiled lead wire designs are used currently to achieve good lead flexibility and to minimize local strains during flexing thereby improving fatigue characteristics. Stainless steel, wrought CoCrMo alloy (Elgiloy) and Co-Ni alloys (MP35N) are popular choices for conducting leads [7].

## 2.24 Dental Alloys

Metals are used in dentistry for direct fillings in teeth (dental amalgams), fabricating crowns and bridges (noble metal and base metal alloys), partial denture frameworks (base metal alloys), orthodontic wires and brackets (stainless steel, Ti alloys

and Ni-Ti alloys) and dental implants (CP Ti and Ti6Al4V). As in the orthopedic applications, the major advantage of metal for these dental applications is the high intrinsic strength and fracture resistance of this class of materials. Biocompatibility is again an important requirement since these materials also contact body tissues (tooth structure, soft supportive tissues) often for the remainder of a patient's lifetime although the ease of accessibility after placement relaxes the biocompatibility requirement considerably. A number of the metals already described (as indicated above) find application in dentistry. Dental implant materials with requirements very similar to materials used for orthopedic joint replacement implants are made almost exclusively from Ti and Ti6Al4V. Orthodontic wires and brackets are made of stainless steel (types 302, 303, 304 and 305), CoCrNiMo alloys (Elgiloy),  $\beta$ -Ti, and Ni-Ti alloys (because of their low elastic moduli, high strengths and consequently large working range, a desirable characteristic for this application).

## 2.25 Dental Amalgams

Dental amalgams are formed by adding Hg to dental amalgam alloys (alloys containing Ag, Cu and Sn plus some other minor elemental additions) (amalgamation process) [33]. Dental amalgam alloys are either low (Cu <6 wt%) or high Cu-containing (Cu >6 wt%), the latter being favored because it avoids the formation of an undesirable Sn-Hg phase ( $\gamma_2$ ) that is susceptible to corrosion and results in lower strength properties of amalgams. Dental amalgam alloys are formed as powders either by lathe cutting Ag-Cu-Sn alloy billets (resulting in irregular particles – i.e., machining chips) or by atomization (to give spherical powders). Subsequent mixing of these alloy powders with liquid mercury results in their partial dissolution, complete consumption of the liquid Hg and the subsequent formation of a number of intermetallic compounds ( $\text{Ag}_3\text{Sn}$ ,  $\text{Ag}_2\text{Hg}_3$ ,  $\text{Sn}_{7-8}\text{Hg}$ ,  $\text{Cu}_3\text{Sn}$ ,  $\text{Cu}_6\text{Sn}_5$ ) due to the Hg-dental amalgam alloy reactions and the condensation of the initial 'plastic' mass to form a load-bearing filling. During the reaction, the partially reacted powder can be manipulated to fill a tooth cavity. The final amalgam restoration exhibits reasonable mechanical properties. While susceptible to corrosion in the oral environment, buildup of the corrosion product serves to limit the rate of further corrosion and to form an acceptable marginal seal at the amalgam-tooth interface. The major advantage of this material is its easy in situ formability to a desired shape. Concerns related to Hg toxicity have been raised but, to date, these have not been proven to be valid although the issue remains controversial.

## 2.26 Dental Casting Alloys – (Au-based, Co- and Ni-based, Ti-based)

Dental casting alloys are used for making dental bridges, crowns (with porcelain fused to a metal substrate), inlays, onlays, and endodontic posts. Both noble and non-noble (base) metal alloys are used to form these often complex shapes.

**Table 2.9** Dental casting alloys [7]

Alloy type	Ag	Au	Cu	Pd	Pt	Zn	Other	
<b>High noble</b>								
Au-Ag-Pt	11.5	78.1	–	–	9.9	–	Ir (trace)	
Au-Cu-Ag-Pd- <i>I</i>	10.0	75.0	10.5	2.4	0.1	1.0	Ru (trace)	
Au-Cu-Ag-Pd- <i>II</i>	25.0	56.0	11.8	5.0	0.4	1.7	Ir (trace)	
<b>Noble</b>								
Au-Cu-Ag-Pd- <i>III</i>	47.0	40.0	7.5	4.0	–	1.5	Ir (trace)	
Au-Ag-Pd-In	38.7	20.0	–	21.0	–	3.8	In 16.5	
Pd-Cu-Ga	–	2.0	10.0	77.0	–	–	Ga 7.0	
Ag-Pd	70.0	–	–	25.0	–	2.0	In 3.0	
<b>Base metal</b>	<b>Ni</b>	<b>Cr</b>	<b>Co</b>	<b>Ti</b>	<b>Mo</b>	<b>Al</b>	<b>V</b>	<b>Other</b>
Ni-Cr	69–77	11–20	–	–	4–14	0–4	–	Fe, Be, Ga, Mn, B
Co-Cr	–	15–25	55–58	–	0–4	0–2	–	Fe, Ga, Nb, W, B, Ru
Ti	–	–	–	90–100			0–4	

Requirements include sufficient strength, toughness, wear resistance, corrosion resistance and biocompatibility. The noble metal alloy compositions are primarily Au- or Pd-based with alloying additions of Ag, Cu, Pt, Zn and some other trace elements. These can be divided into ‘high noble’ alloys (noble metal content  $\geq 60$  wt%) and ‘noble’ alloys (noble metal content  $\geq 25$  wt%) [7]. Some of the Au-based alloys are heat treatable with precipitation hardening or order-disorder reactions (similar effect to precipitation hardening for some alloys) contributing to increased strengths. The base (non-noble) metal alloys contain  $\leq 25$  wt% noble metal elements and are either CoCr or NiCr alloys (Table 2.9). Cast Ti components for crowns, partial and complete dentures, while limited because of difficulties associated with casting because of the high melting point of Ti (compared to Au-based dental alloys), its high reactivity, difficulty in surface finishing and other problems, can be made (using special vacuum melting and casting equipment) but it is not common. Such cast Ti components are useful, however, for individuals with allergies to Ni- or Co-based alloys. Cast Ti-based alloys are also possible including Ti6Al4V, TiCuNi, TiV, TiCu, TiPd and TiCo alloys (some of these are still in the experimental stage of development). To satisfy esthetic requirements for dental crowns, porcelain-fused-to-metal (PFM) restorations are made with the silicate-based porcelains being bonded to a cast metal substrate. Attainment of good bonding of porcelain to the dental alloy substrate is achieved through micromechanical interlock and interfacial chemical reactions, the latter usually involving a substrate surface oxide reacting with the porcelain coating. Compatible thermal expansion coefficients of metal coping and porcelain cladding materials are important to ensure slight residual compressive stresses in the porcelain for inhibition of cracking. Corrosion resistance of the underlying dental alloy is necessary to avoid unacceptable staining and discoloration of a PFM crown.

## 2.27 Wrought Dental Alloys

As noted previously, wrought stainless steel, CoCrNi (Elgiloy),  $\beta$ -Ti and Nitinol alloys are used for making orthodontic wires where high yield strength and preferably low elastic modulus provide high 'working range' characteristics. The requirement of low elastic modulus favors the selection of  $\beta$ -Ti and Ni-Ti alloys for orthodontic wires although all four alloys are used at present. Wire drawing procedures result in strain hardening and high yield strengths but can be performed such that the wires are sufficiently ductile to allow their manipulation and shaping during placement.

CP Ti and ( $\alpha + \beta$ ) Ti alloys (Ti6Al4V) are used for making endosseous dental implants. These components are prepared by machining shapes from bar stock followed by appropriate surface finish operations. In order to achieve more rapid osseointegration, implant surfaces are modified using plasma spray coating, acid etching, grit blasting, laser ablation or addition of metal powder sintered surface layers [34]. These additional treatments can result in final products with either mill-annealed microstructures or, as in the case of Ti6Al4V implants with sintered surface layers,  $\beta$ -annealed structures. In addition to geometric or topographic surface modifications, surface chemical modifications (addition of calcium phosphate surface layers using one of a number of possible methods) are used to promote increased osteoconductivity resulting in faster rates of osseointegration.

## 2.28 New Directions

The metals and alloys used for forming biomedical implants to date have consisted of conventional polycrystalline structures. Methods of formation, as noted previously, have involved casting, forging, milling, machining and honing, metal powder compaction and sintering including the new approach of metal injection molding (MIM) to form near net-shape parts, hot isostatic pressing as well as other conventional metal processing methods (wire drawing, rolling, extrusion and so on). All these result in metallic microstructures with grains in the micron to millimeter size range. In order to achieve preferred mechanical properties grain refinement, alloy additions, strain hardening, development of multi-phase structures and precipitation hardening are used to achieve high strength with acceptable ductility, and fatigue strength in particular, for highly loaded components. Wear resistance of these conventional metals is dependent on the formation of hard non-metallic phases ( $M_{23}C_6$  for example) or surface modification through ion implantation or physical vapor deposition (PVD) of hard non-metallic surface layers. Corrosion resistance for all but the noble metals relies on formation of stable passive oxide layers. Over the past 20–30 years there have been increasing studies on the formation of nanocrystalline (grain size  $< 100$  nm) and amorphous (glassy) metals for various applications. Much higher yield strength, wear resistance and corrosion resistance has been shown for some pure metals formed with such fine microstructures. The higher strengths are explained by the greater resistance to mechanical deformation due to inability for

dislocation movement within the nanoscale crystals. Studies on optimizing structures to achieve high strength and hardness with a required degree of ductility have involved the use of bimodal grain size distributions, with nanocrystalline and some microcrystalline regions [35]. The much greater hardness of the nanocrystalline metals suggest their potential as surface coatings for achieving better wear resistance than conventional alloys without the potential disadvantage of hard non-metallic particles that might become dislodged forming hard 3rd body wear particles. Improved corrosion resistance has also been observed with nanocrystalline metals. While the reason for this improved corrosion resistance is not fully understood, it is suggested that this may be due to reduced electrochemical potentials between anodic and cathodic zones within the nanocrystalline structures [36]. In effect the anodic intergranular and the cathodic intragranular regions are less distinct in the refined structure so the driving potential for corrosion is reduced. More rapid re-passivation due to the high grain boundary area has also been proposed as a reason for the enhanced corrosion resistance.

Methods that have been reported for forming nanocrystalline and amorphous metals and coatings involve rapid melt cooling rates ( $\sim 10^6$  °C/s) through atomization or melt spinning methods, extreme mechanical deformation to give heavy mechanical deformation followed by recrystallization anneals to yield high nucleation rates with limited grain growth, mechanical attrition or milling of gas atomized powders followed by plasma spraying (for coatings), pulsed electrodeposition and other PVD and CVD methods (for coatings and possibly bulk components). In addition to developing very fine grain structures, some of these approaches also offer the possibility of unique non-equilibrium phases forming at room temperature. The determination of the properties of the novel compositions and structures possible by these methods (including their biocompatibility characteristics) presents an exciting area for future biomaterials research.

## References

1. Ashby MF and Jones DR. Engineering Materials 1. An Introduction to their Properties and Applications, and 2. An Introduction to Microstructures, Processing and Design, Pergamon Press: London, 1980.
2. Newey C and Weaver G. Materials Principles and Practice, Butterworth Scientific Ltd.: Guildford 1990.
3. Callister WD Jr. Materials Science and Engineering: An Introduction, 6th ed, Chapter 7, John Wiley & Sons, Inc, 2003.
4. Wayman CM and Duerig TW. An introduction to martensite and shape memory, in Duerig TW, Melton KN, Stockel, D, and Wayman, CM, eds. Engineering Aspects of Shape Memory Alloys, 1990, pp. 3–20.
5. Pilliar RM. Modern metal processing for improved load-bearing surgical implants. *Biomaterials*, 1991, 12: 95–100.
6. Williams DF. Corrosion of orthopedic implants, in Williams DF, ed. *Biocompatibility of Orthopedic Implants*, Vol 1, chap. 6, CRC Press: Boca Raton, FL, 1982.
7. Davis JR, ed. Metallic Materials, Chapter 3, in *Handbook of Materials for Medical Devices*, ASM International, Materials park, Ohio, USA, 2003.
8. Pilliar RM and Weatherly GC. Developments in implant alloys, *CRC Critical Reviews in Biocompatibility*, Vol 1, 1986, pp. 371–403.

9. Sigwart U. Endoluminal Stenting, WB Saunders Co Ltd: London, UK, 1996.
10. Tandon R. Ne-shaping of Co-Cr-Mo (F75) via Metal Injection Molding, in Disegi JA, Kennedy RL, and Pilliar R, eds. Cobalt-Base Alloys for Biomedical Applications, ASTM STP 1365, American Society for Testing and Materials: West Conshohocken, PA, 1999, pp. 3–10.
11. Kilner T, Laanemae WM, Pilliar RM, Weatherly GC, and MacEwen SR. Static mechanical properties of cast and sinter-annealed cobalt-chromium surgical implants, *J Mater Sci*, 1986, 21: 1349–1356.
12. Taylor RNJ and Waterhouse RB. A study of aging behaviour of a cobaltbased implant alloy, *J Mater Sci*, 1983, 18:3265–3280.
13. Kilner T, Pilliar RM, Weatherly GC, and Allibert C. Phase identification and incipient melting in a cast co-Cr surgical implant alloy. *J Biomed mater Res*, 1982, 16:63–79.
14. Wang KK. A dispersion strengthened Co-Cr-Mo alloy for medical implants, in Disegi JA, Kennedy RL, Pilliar R, eds. Cobalt-Base Alloys for Biomedical Applications, ASTM STP 1365, American Society for Testing and Materials West: Conshohocken, PA, 1999, pp. 89–97.
15. Berlin RM, Gustavson LJ, and Wang KK. Influence of post processing on the mechanical properties of investment cast and wrought Co-Cr-Mo alloys, in Disegi JA, Kennedy RL, Pilliar R, eds. Cobalt-Base Alloys for Biomedical Applications, ASTM STP 1365, American Society for Testing and Materials: West Conshohocken, PA, 1999, pp. 62–70.
16. Mishra AK, Hamby MA, and Kaiser WB. Metallurgy, microstructure, chemistry and mechanical properties of a new grade of cobalt-chromium alloy before and after porous-coating, in Disegi JA, Kennedy RL, Pilliar R, eds. Cobalt-Base Alloys for Biomedical Applications, ASTM STP 1365, American Society for Testing and Materials: West Conshohocken, PA, 1999, pp. 71–88.
17. Pilliar RM. Powder metal-made orthopaedic implants with porous surfaces for fixation by tissue ingrowth, *Clin Orthop Rel Res*, 1983, 176:42–51.
18. Pilliar RM. Porous-surfaced metallic implants for orthopedic applications, *J Biomed Mater res*, 1987, A1:1–33.
19. Ankem S and Seagle SR. Heat treatment of metastable beta titanium alloys, in Rosenberg H and Boyer RR, eds. Beta Titanium Alloys in the 1980's, AIME: New York, 1984, pp. 107–126.
20. Long M and Rack HJ. Titanium alloys in total joint replacement – a materials science perspective, *Biomaterials*, 1998, 19:1621–1639.
21. Yue S, Pilliar RM, and Weatherly GC. The fatigue strength of porous-coated Ti-6Al-4 V implant alloy. *J Biomed Mat Res*, 1984 18: 1043.
22. Bania PJ. Beta titanium alloys and their role in the titanium industry, in Eylon D, Boyer RR and Koss DA, eds. Beta Titanium Alloys in the 1990's, The Minerals, Metals & Materials Soc.: Warrendale, PA, 1993, pp. 3–14.
23. Mishra AK, Davidson JA, Poggie RA, Kovacs P, and Fitzgerald TJ. Mechanical and tribological properties and biocompatibility of diffusion hardened Ti- 13Nb-13Zr – A new titanium alloy for surgical implants, in Medical Applications of Titanium and its Alloys: The Material and Biological Issues ASTM STP1272, 1996, pp. 96–113.
24. Benezra V, Mangin S, Treska M, Spector M, Hunter G, and Hobbs LW. Microstructural investigation of the oxide scale of Zr-2.5Nb and its interface with the alloy substrate, in Biomedical Materials-Drug Delivery, Implants and Tissue Engineering, *Mater Res Soc Symp Proc*, 1999, 550: 337–342.
25. Haasters J, v Salis-Salio G, and Bensmann G. The use of Ni-Ti as an implant in orthopaedics, in Deurig TW, Melton KN, Stockel D, and Wayman CM, eds. Engineering Aspects of Shape Memory Alloys, 1990, pp. 426–444.
26. Wever DJ, Veldhuizen AG, Sanders MM, Schakenrad JM, and van Horn JR. Cytotoxic, allergic and genotoxic activity of a nickel-titanium alloy. *Biomaterials*, 1997, 18:1115–1120.



27. Kapanen A, Ryhanen J, Danilov A, and Tuukkanen J. Effect of nickel-titanium shape memory alloy on bone formation. *Biomaterials*, 2001, 22: 2475–2480.
28. Firstov GS, Vitchev RG, Kumar H, Blanpain B, and Van Humbeeck J. Surface oxidation of NiTi shape memory alloy. *Biomaterials*, 2002, 23:4863–4871.
29. Cisse O, Savadogo O, Wu M, and Yahia LH. Effect of surface treatment of NiTi alloy on its corrosion behavior in Hanks' solution. *J Biomed Mater Res*, 2002, 61: 339–345.
30. Assad M, Chernyshov AV, Jarzem P, Leroux MA, Coillard C, Charette S, and Rivard C-H. Porous titanium-nickel for intervertebral fusion in a sheep model: Part 2. Surface analysis and nickel release assessment. *J Biomed Mater Res Pt B: Appl Biomater*, 2003, 64B:121–129.
31. Zardiackas LD, Parsell DE, Dillon LD, Mitchell DW, Nunnery LA, and Poggie R. Structure, metallurgy and mechanical properties of a porous tantalum foam. *J Biomed Mater Res (Appl Biomater)*, 2001, 58:180–187.
32. Boby JD, Stackpool GJ, Hacking SA, Tanzer M, and Krygier JJ. Characteristics of bone ingrowth and interface mechanics of a new porous tantalum biomaterial. *J Bone Jt Surg*, 1999, 81-B: 907–914.
33. Phillip's Science of Dental Materials, in Anusavice KJ, ed. *Dental Amalgam: Structures and Properties*, chap 17, 10th Edition, 1996.
34. Pilliar RM. An Overview of Surface Variability of Metallic Endosseous Dental Implants: Textured and Porous surface-Structured Designs. *Implant Dent*, 1998, 7: 305–314.
35. Baker SP. Plastic deformation and strength of materials in small dimensions. *Mat Sci Eng*, 2001, 319–321: 16–23.
36. Cheng D, Tellkamp VL, Lavernia CJ, and Lavernia EJ. Corrosion properties of nanocrystalline Co-Cr coatings. *Ann Biomed Eng*, 2001, 29: 803–809.



<http://www.springer.com/978-0-387-84871-6>

Biomedical Materials

Narayan, R. (Ed.)

2009, XXIII, 566 p., Hardcover

ISBN: 978-0-387-84871-6